Toxoplasma gondii Infection Drives Conversion of NK Cells into ILC1s

Eugene Park,[1] Swapneel J. Patel,[1] Qiuling Wang,[2] Prabhakar S. Andhey,[3] Konstantin Zaitsev,[3,4] Sofia I. Porter,[3] Maxwell L. Hershey,[1] Michael D. Bern,[1] Beatrice Plougastel-Douglas,[1] Patrick L. Collins,[3] Marco Colonna,[3] Kenneth M. Murphy,[3] Eugene M. Oltz,[3,5] Maxim N. Artyomov,[3] L. David Sibley,[2] and Wayne M. Yokoyama[1]

[1]Division of Rheumatology, Department of Medicine, Washington University School of Medicine, St. Louis, MO 63108, USA

[2]Department of Molecular Microbiology, Washington University School of Medicine, St. Louis, MO 63108, USA

[3]Department of Pathology and Immunology, Washington University School of Medicine, St. Louis, MO 63108, USA

[4]Computer Technologies Department, ITMO University, Saint Petersburg, Russia

[5]Department of Microbial Infection and Immunity, Ohio State University Wexner School of Medicine, Columbus, OH 43210, USA

*Correspondence: yokoyama@wustl.edu

Abstract

Innate lymphoid cells (ILCs) were originally classified based on their cytokine profiles, placing natural killer (NK) cells and ILC1s together, but recent studies support their separation into different lineages at steady-state. However, tumors may induce NK cell conversion into ILC1-like cells that are limited to the tumor microenvironment and whether this conversion occurs beyond this environment remains unknown. Here we describe *Toxoplasma gondii* infection converts NK cells into cells resembling steady-state ILC1s that are heterogeneous and distinct from both steady-state NK cells and ILC1s in uninfected mice. Most toxoplasma-induced ILC1s were Eomes-dependent, indicating that NK cells can give rise to Eomes$^-$ Tbet-dependent ILC1-like cells that circulate widely and persist independent of ongoing infection. Moreover, these changes appear permanent, as supported by epigenetic analyses. Thus, these studies markedly expand current concepts of NK cells, ILCs, and their potential conversion.

Introduction

Innate lymphoid cells (ILCs) comprise diverse populations. Like T and B cells, they are derived from common lymphoid progenitors (CLPs) but do not undergo antigen receptor recombination (Spits and Cupedo, 2012). ILCs are tissue-resident within mucosal sites where they participate in tissue homeostasis and survey for pathogens (Sojka et al., 2014a, Gasteiger et al., 2015), although recent studies showed that inflammation can induce ILC2 mobilization (Huang et al., 2018). ILC classification was initially based on their cytokine production, with type 1 ILCs (ILC1s) producing IFNγ, ILC2s producing IL-5 and IL-13, and ILC3s producing IL-17 and IL-22. ILC classification was subsequently corroborated by distinctive markers and developmental requirements.

Prior to the discovery of ILCs, NK cells were the only known innate CD3$^-$ lymphocytes. Their classification within the larger scheme of ILCs has been challenging, in particular due to their strong resemblance to ILC1s while also maintaining important distinctions. For example, mouse ILC1s and NK cells both express NK1.1 and NKp46 and produce IFNγ, and as such were initially classified together as Group 1 ILCs (Spits et al., 2013). However, grouping NK cells with ILC1s was confounded by several discordant features.

Whereas ILC1s are restricted to organs, and CD49a expression is a faithful marker of tissue-resident populations under steady-state conditions (Peng et al., 2013, Sojka et al., 2014a), most NK cells freely circulate. These cells also differ in their developmental requirements, with NK cells requiring Eomes for development, while Eomes is not expressed in ILC1s and is dispensable for development (Daussy et al., 2014). Moreover, ILC1s are completely Tbet-dependent (Daussy et al., 2014, Sojka et al., 2014a), whereas NK cells require Tbet only for maturation (Townsend et al., 2004, Gordon et al., 2012). Consistent with their differential requirements for T-box transcription factors, NK cells and ILC1s arise at different branch points downstream of the CLP. While NK cells originate from NK cell precursor cells (Rosmaraki et al., 2001), other ILCs further differentiate along a pathway that includes the common helper innate lymphoid progenitor (CHILP) and ILC precursor (ILCP), which do not have NK cell potential (Klose et al., 2014, Constantinides et al., 2014, Yang et al., 2015). Given the many ways in which NK cells and ILC1s differ, ILC classification was recently revised so that NK cells and ILC1s are now considered distinct ILC lineages (Vivier et al., 2018).

Constructing clear definitions of NK cells and ILC1s is complicated, however, by their plasticity and heterogeneity upon stimulation, which can alter the features that discriminate between them under steady state conditions. For example, within the tumor microenvironment or upon *in vitro* culture with TGF-β, NK cells may downregulate Eomes and resemble ILC1s (Gao et al., 2017, Cortez et al., 2016). However, these cells are found only in the tumor microenvironment *in vivo* and it is not clear if they can persist in the absence of tumor. Moreover, NK cells and ILC1s become activated under similar circumstances, such as murine cytomegalovirus (MCMV) infection and tumorigenesis (Weizman et al., 2017, Dadi et al., 2016, Yokoyama, 2013). As it is currently difficult to assess NK cells independently of ILC1s, changes undergone by either population may be masked by the presence of the other. Independent examination of each population, especially in settings known to stimulate NK cells and ILC1s, is required to better understand these cells and their relationship to each other.

Both NK cells and ILC1s respond to infection with *Toxoplasma gondii*, an intracellular parasite that infects a third of the global population, and is a natural pathogen in mice (Montoya and Liesenfeld, 2004). During acute infection, rapidly replicating tachyzoites disseminate systemically, triggering dendritic cells to produce IL-12, which subsequently stimulates NK cells to produce IFNγ and ILC1s to produce IFNγ and TNFα (Klose et al., 2014, Goldszmid et al., 2012). Tachyzoites eventually differentiate into slowly replicating bradyzoites, which are primarily encysted within cells of the central nervous system and skeletal muscle (Yarovinsky, 2014). As *T. gondii* infection elicits activation of both NK cells and ILC1s, herein we sought to investigate how NK cells and ILC1s respond to gain better insight into inflammation-induced changes. Indeed, we found that ILC1s become permanently heterogeneous after infection, largely owing to the surprising conversion of NK cells into ILC1s.

Results

T. gondii infection results in ILC1 expansion.

Following administration of α-NK1.1, acute infection with the type II Prugniaud (Pru) strain of *T. gondii* resulted in increased parasite load and higher mortality rates (**Supplementary Fig. 1a-c**), consistent with previous reports (Goldszmid et al., 2007). Since α-NK1.1 affects both NK cells and ILC1s and both of have been previously implicated in the immune response to *T. gondii* (Goldszmid et al., 2012, Klose et al., 2014), we sought to investigate how NK cells and ILC1s respond to infection. Here we assessed these populations by following expression of Eomesodermin (Eomes) and CD49a among $CD3^-$ $CD19^-$ $NK1.1^+$ $NKp46^+$ cells, as NK cells express Eomes and not CD49a while ILC1s express CD49a but not Eomes. In the uninfected spleen, the vast majority of $NK1.1^+$ $NKp46^+$ cells were NK cells (**Fig. 1a**), although there was a small population of ILC1s, which are primarily found in other organs including the liver and small intestine (Sojka et al., 2014a, Fuchs et al., 2013). Interestingly, over the course of infection, NK cells decreased both as a proportion of $NK1.1^+$ $NKp46^+$ cells and in absolute number (**Fig. 1a,b**). By contrast, there was an increase in ILC1s that was clearly evident at 21 d post-infection (p.i.) (**Fig. 1a,c**). Notably, most ILC1s from infected mice expressed Ly6C, unlike ILC1s present under steady state conditions (**Fig. 1a,d**). The expansion of splenic ILC1s persisted for at least 4 months p.i. (**Fig. 1e**).

ILC1 expansion persists in the absence of ongoing infection.

Two major possibilities could account for the sustained expansion of ILC1s. They may represent a response to ongoing parasite replication, as bradyzoites develop following acute infection with Pru *T. gondii* infection and parasite reactivation can occur. Alternatively, the increased ILC1s might be a permanent change that persists even after infection subsides. To test whether ongoing parasite replication plays a role, we infected mice with *T. gondii*, then suppressed growth of tachyzoites with sulfadiazine at various time points p.i. (Eyles and Coleman, 1955). Interestingly, infection induced expansion of ILC1s, as seen at 35 d.p.i, even in sulfadiazine-treated mice when treatment began 7 or 10 d.p.i., with ILC1 numbers comparable to those of untreated, infected mice (**Fig. 2a**). ILC1 expansion also occurred following repeated administration of the *Cps1-1 T. gondii* strain (**Fig. 2b**), which does not replicate *in vivo* and therefore does not persist in a chronic form (Fox and Bzik, 2002). Moreover, the ILC1 number was similar after infection with a single inoculum of Δgra4 parasites, which are defective in cyst formation (Fox et al., 2011, Jones et al., 2017), as compared to the WT parental Pru strain (**Fig. 2c**). BALB/c mice, which have fewer cysts during chronic *T. gondii* infection (Suzuki et al., 1993), also had increased numbers of ILC1s after Pru infection (**Fig. 2d**), also indicating that expanded ILC1s were not confined to infected C57BL/6 mice. In summary, we found that *T. gondii* infection induced ILC1 expansion, which persisted independent of ongoing parasite replication, suggesting a permanent change in ILC1s; in subsequent experiments we further examined the impact of infection with the Pru strain of *T. gondii*.

Expansion of ILC1s among circulating cells.

ILC1s have previously been established as being tissue-resident under steady state conditions (Gasteiger et al., 2015, Sojka et al., 2014a, Peng et al., 2013). However, surprisingly, we found that infected mice displayed ILC1 expansion even in the blood, and a highly vascularized organ, i.e., the lung, indicating that at least some of these cells circulate (**Fig. 3a,b**). Consistent with our previous findings in the spleen (**Fig. 1a,d**), the ILC1s in the blood and lungs of infected mice also expressed Ly6C (**Supplementary Fig. 2a**).

However, there was no increase of ILC1s in the mesenteric lymph node, brain, peritoneum, bone marrow, uterus, or salivary gland (**Fig. 3c**, **Supplementary Fig. 2b**). Nonetheless, these data indicated that *T. gondii* infection induced ILC1 expansion, even in the circulation.

Parabiosis experiments could provide supportive evidence of circulating versus tissue-resident cells, but the possible reactivation and spread of *T. gondii* following surgery, as seen clinically (Bosch-Driessen et al., 2002), could confound analysis. Instead, we utilized *Eomes*-GFP reporter mice to assess how ILC1s and NK cells from infected mice behave following transfer into uninfected mice (Daussy et al., 2014). We isolated NK cells and ILC1s from congenically distinct *Eomes-GFP* mice 35 d.p.i. for adoptive transfer into naïve *Rag2*$^{-/-}$ *Il2rg*$^{-/-}$ mice (**Fig. 3d**). When we assessed the recipient mice 24 d later, we detected both transferred populations in the spleen and liver (**Fig. 3e**). Although NK cells upregulated CD49a upon transfer into *Rag2*$^{-/-}$ *Il2rg*$^{-/-}$ mice, as previously reported (Gao et al., 2017), the Eomes expression generally remained the same (**Fig. 3f**). Therefore, in the setting of homeostatic expansion, transferred NK cells and ILC1s from infected mice persist with generally stable Eomes expression, and transferred ILCs from infected mice can circulate, providing complementary evidence, in addition to above (**Fig 2a-d**), that they persist in the absence of ongoing infection.

Interestingly, however, the ratio of transferred ILC1s to NK cells was higher in the liver than in the spleen, with ILC1s comprising nearly all transferred cells in the liver (**Fig. 3e**). This suggested that the ILC1s from infected mice may not uniformly circulate and rather they might preferentially migrate to the liver despite originating in the spleen. Alternatively, the adoptive transfer studies may be revealing properties of heterogeneous populations of cells. To further evaluate these issues, we studied the liver, which contains a much larger population of ILC1s than the spleen, in more detail directly following primary infection. Infection decreased the frequency of liver NK cells among NK1.1^{+} NKp46^{+} cells, though the total NK cell number did not change (**Fig. 3g,h)**. Notably, we observed that infection resulted in a striking population of liver Eomes^{+} CD49a^{+} cells (**Fig. 3g,i**). The frequency and absolute number of ILC1s also did not change (**Fig. 3j**), although this was potentially confounded by the sizeable ILC1 population already present at

steady state (Sojka et al., 2014a, Peng et al., 2013). Indeed, we found that Ly6C was expressed by only half of the ILC1s in the livers of infected mice at 35 d.p.i. (**Fig. 3g,k**) while Ly6C was expressed by a higher percentage (~80%, **Fig 1d**). Accordingly, the number of liver Ly6C$^+$ ILC1s was increased relative to uninfected mice, whereas the number of Ly6C$^-$ ILC1s remained comparable (**Fig. 3k**). This suggested that at 35 d.p.i. not all ILC1s displayed effects of *T. gondii* infection and that Ly6C expression may distinguish between steady-state ILC1s and ILC1s induced by infection. Thus, the data suggest that in infected mice, steady-state ILC1s are maintained while an additional ILC1 subset arises.

T. gondii-induced ILC1s are distinct from NK Cells and ILC1s.

Ly6C is expressed by ILC1s only in the spleen, blood, and liver of infected mice, raising the possibility that *T. gondii* induces the development of ILC1s that do not exist under steady state conditions. To assess the possibility of a novel ILC1 subset, we first performed more detailed comparisons of NK cells and ILC1s in the spleens of uninfected and infected mice. As circulatory capacity was specific to ILC1s in infected mice, we examined expression of molecules typically associated with ILC1 tissue-residency (Sojka et al., 2014a, Daussy et al., 2014). ILC1s in both uninfected and infected mice did not express CD62L and expressed higher levels of PECAM-1 and CXCR6 compared to NK cells (**Fig. 4a**). However, infection resulted in NK cells and ILC1s gaining expression of CCR8 and CX_3CR1 compared to NK cells and ILC1s in uninfected mice. Additional differences included ILC1s from infected mice expressing Neuropilin-1 and KLRG1 at higher levels than other populations, and DNAM-1 more highly than NK cells (**Fig. 4b**). Moreover, while ILC1s from uninfected mice were predominantly CD27$^+$ CD11b$^-$ and NK cells from uninfected and infected mice encompassed all subsets, ILC1s from infected mice were mainly CD27$^-$ CD11b$^+$ (**Fig. 4c**). Most ILC1s in both uninfected and infected mice expressed NKG2A and expressed Ly49 receptors at low frequencies (**Fig. 4d**). NK cells also displayed decreased frequency of Ly49D$^+$ and Ly49H$^+$ subsets following infection. Lastly, NK cells and ILC1s in both uninfected and infected mice produced IFNγ in response to stimulation (**Fig. 4e**), a hallmark of both cell types (Sojka et al., 2014b). However, only ILC1s from uninfected mice could produce TNFα (**Fig. 4f**). Similar results were

obtained from studies of ILC1s in blood of infected mice (**Supplementary Fig. 3a,b**). Thus, the spleens and blood of infected mice contained a novel ILC1 subset.

Studies of the infected liver solidified the notion that infection induced the formation of a distinct ILC1 subpopulation. In the liver, we separately assessed the Ly6C$^-$ ILC1s that are present in uninfected mice, as well as both Ly6C$^-$ ILC1s and Ly6C$^+$ ILC1s in infected mice (**Supplementary Fig. 3c**). Ly6C$^+$ ILC1s expressed higher levels of CX_3CR1, Neuropilin-1, KLRG1, and CD11b, lower levels of CXCR6 and CD27, and produced less TNFα than Ly6C$^-$ ILC1s in uninfected and infected mice, which were similar (**Supplementary Fig. 3d-f**). Therefore, the Ly6C$^+$ ILC1s in the liver therefore resembled those in the infected spleen (**Fig. 4a-c,f**), suggesting that while ILC1s in uninfected and infected mice share the Eomes$^-$ CD49a$^+$ phenotype, they can be distinguished by marker expression and cytokine production profile.

T. gondii infection induces heterogeneity of NK Cells and ILC1s.

ILC1s in infected mice expressed high levels of Tbet (**Fig. 5a**), which was previously identified as a requirement for ILC1 development (Daussy et al., 2014, Sojka et al., 2014a). We therefore hypothesized that Tbet may be required for ILC1 expansion after infection. As *Tbx21*$^{-/-}$ mice succumb to *T. gondii* infection (Harms Pritchard et al., 2015), we studied WT:*Tbx21*$^{-/-}$ mixed bone marrow chimeras. In spleens of both uninfected and infected chimeras, NK cells were present though they were biased towards WT origin (**Fig. 5b**, **Supplementary Fig. 4a)**, consistent with a requirement for Tbet to complete NK cell maturation (Gordon et al., 2012). However, no ILC1s (Eomes$^-$ CD49a$^+$) were found of *Tbx21*$^{-/-}$ origin in infected WT:*Tbx21*$^{-/-}$ chimeras, as with ILC1s in naïve chimeras. Thus, splenic ILC1s are Tbet-dependent, even after *T. gondii* infection.

In the livers of infected WT:*Tbx21*$^{-/-}$ chimeras, the picture was more complex. There were no ILC1s (Eomes$^-$ CD49a$^+$) of *Tbx21*$^{-/-}$ origin in the infected liver, as with infected spleens (**Fig. 5b**). However, the livers of infected WT:*Tbx21*$^{-/-}$ chimeras displayed an accumulation of *Tbx21*$^{-/-}$ Eomes$^+$ CD49a$^+$ cells that

were not present in the spleen (**Fig. 5b**). Eomes^{+} CD49a^{+} cells were also present among counterpart WT cells, though at lower frequencies. These data suggested that ILC1s in infected mice may be derived from Eomes^{+} cells, i.e., NK cells.

To better assess the heterogeneity induced by *T. gondii* infection and the role of Tbet in this process, we performed single-cell RNA-seq (scRNA-seq) on sorted WT (CD45.1^{+}) or *Tbx21*$^{-/-}$ (CD45.2^{+}) NK1.1^{+} NKp46^{+} cells from uninfected and d35-infected WT:*Tbx21*$^{-/-}$ chimeras. We chose to examine the liver for this analysis for several reasons: 1) infection appears to induce a novel ILC1 subset that is common to the liver and spleen; 2) the liver contains ILC1s under steady state, allowing for direct comparison of steady-state ILC1s and *T. gondii*-induced ILC1s; and 3) the infected liver uniquely contains a *Tbx21*$^{-/-}$ Eomes^{+} CD49a^{+} population. Using t-distributed stochastic neighbor embedding (t-SNE) analysis, we grouped the cells into 17 clusters, C1-C17 (**Fig. 5c**). In the uninfected WT sample, C1 was the largest cluster, whereas C1 was diminished in the infected WT and *Tbx21*$^{-/-}$ samples (**Fig. 5d,e**). C1 cells expressed *Eomes* and *Itgam* but did not express *Cd27* or *Itga1* (**Fig. 5f,g**), consistent with C1 being mature NK cells, which are indeed the predominant NK1.1^{+} NKp46^{+} cells present in the steady-state liver (**Supplementary Fig. 5b-d**). C3 was the second largest cluster in the uninfected WT sample, and C3 cells did not express *Eomes* or *Ly6c2*, expressed *Itga1*, *Cd27*, and *Cxcr6*, and were absent in *Tbx21*$^{-/-}$ samples, indicating that C3 comprised ILC1s (**Fig. 5f,g, Supplementary Fig. 4d**).

Two closely related clusters, C10 and C11, were unique to the infected WT sample (**Fig. 5d,e**). Cells in C10 and C11 expressed *Itga1*, *Ly6c2*, and *Klrg1*, and did not express *Eomes* (**Fig. 5f,g)**. This specificity to infection, Tbet-dependence, and gene expression identified these cells as *T. gondii*-induced ILC1s. Interestingly, these two clusters indicated heterogeneity even within the *T. gondii*-induced ILC1 population. The t-SNE analysis placed C10 closer to mature NK cells (C1) and C11 closer to ILC1s (C3). Comparison of C10 and C11 revealed that C10 expressed signature NK cell genes at higher levels (Robinette et al., 2015), whereas C11 expressed higher levels of signature ILC1 genes **(Supplementary Fig. 4e)**. Interestingly, C10 also highly expressed *Cx3cr1* whereas C11 did not (**Fig. 5f,g**). We

corroborated these findings with flow cytometric analysis that showed that Ly6C$^+$ ILC1s in the infected liver contained both a CX$_3$CR1$^+$ CXCR6$^-$ population that expressed higher levels of Zeb2, mirroring the C10 phenotype, and also a CX$_3$CR1$^-$ CXCR6$^+$ population that mirrors C11 (**Supplementary Fig. 4f,g**). C5 was also increased in the infected samples, and these cells co-expressed *Eomes* and *Itga1*, and were especially prominent in the infected *Tbx21*$^{-/-}$ sample (**Fig. 5e,g**), suggesting that this cluster includes the Eomes$^+$ CD49a$^+$ cells that arose in the liver after infection (**Fig. 5b**). In summary, scRNA-seq analysis revealed that *T. gondii* infection induces heterogeneous NK cell and ILC1 populations, including two distinct ILC1 subpopulations that are unique to infected mice.

NK Cells downregulate Eomes during *T. gondii* infection.

scRNA-seq analysis revealed heterogeneity of NK1.1$^+$ NKp46$^+$ cells and showed that some *T. gondii*-induced ILC1s have core NK cell traits. To assess if NK cell conversion into ILC1s might account for this population by means of Eomes downregulation, we examined *Ncr1*^{iCre} *Eomes*$^{f/f}$ (*Eomes* conditional KO or cKO) mice, in which NK cells are absent owing to their requirement for Eomes, as shown by a drastic reduction of NK1.1$^+$ NKp46$^+$ cells (**Supplementary Fig. 5a**) with normal numbers of CD49a$^+$ ILC1s (**Fig. 6a,b**) (Gordon et al., 2012, Pikovskaya et al., 2016). Following *T. gondii* infection, the numbers of CD49a$^+$ and CD49a$^+$ Ly6C$^+$ cells in the spleen were significantly reduced in *Eomes* cKO compared to *Eomes*$^{f/f}$ controls (**Fig. 6a,b**), showing that expansion of these cells requires Eomes. However, while the overall number of CD49a$^+$ cells did not change between uninfected and infected *Eomes* cKO mice, the number of CD49a$^+$ Ly6C$^+$ cells increased slightly (**Fig. 6b**), and a greater frequency of the CD49a$^+$ cells expressed Ly6C (**Fig. 6c**), showing that mild ILC1 expansion occurs in the absence of NK cells. However, approximately three times as many CD49a$^+$ Ly6C$^+$ cells were derived from Eomes-dependent cells, i.e., NK cells (**Fig. 6b**), suggesting Eomes expression by NK cells contributes to the development of most *T. gondii*-induced ILC1s.

The role of Eomes-expressing NK cells in formation of *T. gondii*-induced ILC1s could be either cell-intrinsic or cell-extrinsic. Though an Eomes fate-mapping mouse, i.e., Eomes^{Cre}, could be used to identify

a cell-intrinsic role for Eomes, this was not possible due to the ubiquitous expression of Eomes during development (data not shown). Another approach would be to examine Eomes downregulation following adoptive transfer of congenic NK cells prior to infection but this was hindered due to the inability to find transferred cells after 14 d.p.i. (data not shown), possibly due to the high turnover of cells during infection. Rather, we used mixed bone marrow chimeras to examine a cell-intrinsic or cell-extrinsic requirement for Eomes during *T. gondii*-induced ILC1 expansion. In uninfected mixed bone marrow chimeras reconstituted with WT cells and either *Eomes*$^{f/f}$ or *Eomes* cKO cells, the contributions of *Eomes*$^{f/f}$ and *Eomes* cKO cells to CD49a^{+} cells were comparable, consistent with CD49a^{+} cells being Eomes-independent ILC1s (**Fig. 6d**). This degree of chimerism did not change upon infection of WT:*Eomes*$^{f/f}$ chimeras. However, infection of WT:*Eomes* cKO chimeras resulted in a significant reduction of CD49a^{+} cells of *Eomes* cKO origin. Although there were a few CD49a^{+} ILC1s of *Eomes* cKO origin, consistent with Eomes-independent ILC1 origin, *T. gondii* infection resulted in ILC1s that were mostly dependent on a cell-intrinsic effect of Eomes in NKp46-expressing cells, i.e., NK cells. Therefore most *T. gondii*-induced ILC1s are ex-NK cells.

We postulated that STAT4 may play a role in the expansion of *T. gondii*-induced ILC1s because STAT4 and IL-12 signaling is critical for NK cell and ILC1 activation during *T. gondii* infection (Hunter et al., 1994, Cai et al., 2000, Klose et al., 2014). To test the relevance of this signaling *in vivo*, we infected WT:*Stat4*$^{-/-}$ mixed bone marrow chimeras. Indeed, STAT4-deficient ILC1s were diminished following infection, while chimerism of NK cells and ILC1s remained equal between uninfected and infected chimeric mice (**Fig. 6e**), suggesting that *T. gondii*-induced ILC1s were dependent on STAT4. Additionally, *in vitro* culture of splenocytes from infected mice resulted in an increased frequency of ILC1s following culture in IL-2 and IL-12, compared to culture in IL-2 alone (**Supplementary Fig. 5b**), suggesting that IL-12 may contribute to ILC1 expansion. However, culture of purified NK cells from infected mice did not result in Eomes downregulation (**Supplementary Fig. 5b,c**), showing there may be IL-12 cell-extrinsic effects involved in this conversion. Notably, *T. gondii*-induced ILC1s stably maintained their phenotype after 2 days in

289 culture (**Supplementary Fig. 5d**). Taken together, these results suggest that STAT4 and IL-12 contribute
290 to ILC1 expansion in the context of *T. gondii* infection, with contributions from additional factors as well.
291
292 **Eomes downregulation within NK cells accompanies extensive transcriptional and epigenomic**
293 **changes.**
294 Our scRNA-seq data suggested that *T. gondii* infection drastically rewires NK cells and ILC1s to induce
295 permanent changes. To provide confirmatory evidence, we performed bulk RNA sequencing (RNA-seq)
296 to inform epigenomic analyses, even though we realize that these approaches lose single cell resolution.
297 For this analysis, we used splenocytes, sorted into NK cells (Ly6C$^-$ CD49a$^-$) from uninfected and infected
298 mice, and *T. gondii*-induced ILC1 (Ly6C$^+$ CD49a$^+$) populations, which were accurately identified Eomes$^+$
299 and Eomes$^-$ cells, respectively (**Supplementary Fig. 6a**). With respect to our scRNA-seq analysis, these
300 cells represent Eomes$^+$ (conventional) NK cells from uninfected and infected mice, and *T. gondii*-induced
301 ILC1s (both converted NK cells and Ly6C$^+$ ILC1s, of which most were converted NK cells, **Fig. 5, 6b**).
302 Principal component analysis and hierarchical clustering showed a higher degree of similarity between
303 NK cells from uninfected and infected mice, relative to *T. gondii*-induced ILC1s (**Fig. 7a,b**). As expected,
304 *Ly6c1*, *Ly6c2*, *Itga1*, and *Eomes* were differentially expressed (**Fig. 7c**). We found extensive differences
305 between NK cells and *T. gondii*-induced ILC1s, including differences in the expression of surface
306 markers, transcription factors, secreted factors, adhesion molecules, chemokine receptors, and signaling
307 molecules (**Fig. 7d**).
308
309 Since NK cells and ILC1s display distinct patterns of chromatin accessibility (Shih et al., 2016), and
310 infection can induce long-lasting epigenomic changes in NK cells (Lau et al., 2018), we performed the
311 assay for accessibility for transposase-accessible chromatin using sequencing (ATAC-seq) (Buenrostro et
312 al., 2015) to compare the NK cells and ILC1s present in *T. gondii*-infected mice at the epigenomic level.
313 We found widespread chromatin remodeling in *T. gondii*-induced ILC1s, with *T. gondii*-induced ILC1s
314 clustering separately from NK cells (**Fig. 7e,f**). Most differentially accessible regions fell within intronic and
315 intergenic regions, consistent with categorization as putative enhancers (**Supplementary Fig. 6b**).

We organized differentially accessible regulatory elements (REs) into a non-redundant peak set containing 6 clusters (**Supplementary Fig. 6c**). Clusters 1, 3, and 5 contained REs that were uniquely more accessible in uninfected NK cells, NK cells from infected mice, and *T. gondii*-induced ILC1s, respectively. Clusters 2, 4, and 6 contained REs that were shared between two groups. Cluster 2 encompassed REs that were more accessible in both NK cell groups relative to *T. gondii*-induced ILC1s, and accounted for the largest fraction of peaks, showing that NK cells share many epigenetic features regardless of infection. Somewhat surprisingly, Cluster 4, which contained REs that were more accessible in both NK cells and ILC1s from infected mice relative to uninfected NK cells, was the second largest cluster, suggesting that infection may induce epigenetic changes common to both populations.

We directly compared the REs in Clusters 3 and 5 to identify additional differences between NK cells and *T. gondii*-induced ILC1s following infection. Analysis of transcription factor binding motifs revealed motifs that were significantly enriched in each population, such as NF-κb in Cluster 3, whose motif was present in 13.2% of REs, and Klf4 in Cluster 5, whose motif was present in 25.8% of REs (**Supplementary Fig. 6d**). We also identified the specific loci that contained the most differentially accessible REs, and noted that the presence of more accessible REs generally correlated with greater gene expression. Notably, many of the epigenetic features shared by memory NK cells and memory $CD8^+$ T cells (Lau et al., 2018) were among the loci that gained accessibility in *T. gondii*-induced ILC1s (**Supplementary Fig. 6e**). Among the differentially accessible regions were the *Eomes* and *Tbx21* loci, supporting our data above detailing expression changes of these transcription factors (**Fig. 7g, Supplementary Fig. 6f**). Overall, our data suggest that *T. gondii* induces the conversion of NK cells into ILC1s in a process that encompasses changes in gene expression and chromatin accessibility.

Discussion

Infection with *T. gondii*, a natural mouse pathogen, causes the expansion of a novel ILC1 subpopulation that stably persists even after acute infection resolves. These ILC1s are heterogeneous, due to contributions from both ILC1s and NK cells, though NK cells give rise to most *T. gondii*-induced ILC1s by

means of Eomes downregulation. These findings disrupt current notions surrounding NK cells and ILC1s, which were recently established as discrete ILC lineages (Vivier et al., 2018), and exemplify the limitations of categorizing NK cells and ILC1s based solely on their phenotypes under steady state conditions.

Previous studies indicated that Eomes downregulation may occur in NK cells within the tumor microenvironment (Gill et al., 2012, Gao et al., 2017) and *in vitro* (Cortez et al., 2016). Akin to the intermediate ILC1s (intILC1s) described within tumors (Gao et al., 2017), we found *T. gondii* infection induced Eomes$^+$ CD49a$^+$ NK cells in the liver, which are possibly intermediates between NK cells and ex-NK cells. However, our findings differ in several significant ways. The tumor studies indicated that Eomes$^-$ NK cells were restricted to tumors and emphasized the importance of the microenvironment (Gao et al., 2017, Gill et al., 2012), concluding that within tumors, Eomes downregulation transiently silences NK cells to hamper immunosurveillance (Silver and Humbles, 2017). There was no evidence presented that these Eomes$^-$ cells can circulate, though they proliferate when adoptively transferred into lymphocyte-deficient hosts. Moreover, it is not clear if these cells persist in the absence of tumor. By contrast, *T. gondii*-induced ILC1s are disseminated throughout the circulation, retain the ability to produce IFNγ, do not produce TNFα, and are maintained in the absence of ongoing stimulus.

Our findings further indicate a permanent transformation of *T. gondii*-induced ILC1s rather than a transient response to inflammation, a notion that is further bolstered by the observations that *T. gondii*-induced ILC1s possess a unique gene expression profile. Moreover, *T. gondii* infection induced epigenetic modifications in NK cells and ILC1s, though our analysis did not specifically examine each of the different individual NK and ILC1 subsets we identified by scRNA-seq. However, these modifications were extensive and could not be readily explained by heterogeneity in the *T. gondii*-induced ILC1s that we discovered by scRNA-seq. Nonetheless, our studies go beyond just the differences between tumor-induced and *T. gondii*-induced Eomes downregulation. Our findings indicate that DX5 and CD49a expression to identify NK cells and ILC1s may not always faithfully reflect Eomes expression, as is the

371 case during early *T. gondii* infection. Moreover, although there is clear evidence supporting conversion
372 from NK cells to Eomes^{-} NK cells, such as intILC1s (Gao et al., 2017), there is a general inability to
373 distinguish between preexisting ILC1s and *de novo* converted ILC1s. Indeed, this may explain
374 discrepancies that currently exist within the field, such as the conflicting report that ILC1-like cells confer
375 protection against certain tumors (Dadi et al., 2016). Thus, our studies suggest that ILC1s may be more
376 heterogeneous than currently thought, as they can arise from distinct precursors (Vivier et al., 2018).
377
378 In *T. gondii* infection, IL-12 is critical for NK cell activation (Gazzinelli et al., 1993) and our data suggest
379 that it can have long-lasting effects. This parallels the requirements for development of memory and
380 memory-like NK cells induced by MCMV and cytokine stimulation (Cooper et al., 2009, Sun et al., 2012,
381 Romee et al., 2012). In addition to IL-12 dependence, MCMV-induced memory NK cells and *T. gondii*-
382 induced ILC1s share Ly6C expression, as well as alterations in their receptor repertoire, although *T.*
383 *gondii*-induced ILC1s primarily express the inhibitory receptor NKG2A while MCMV-induced memory NK
384 cells are Ly49H^{+}. Moreover, memory and memory-like NK cells have few markers that differentiate them
385 from resting NK cells, whereas NK cells converted by *T. gondii* infection lose expression of Eomes and
386 gain expression of Ly6C, KLRG1, CX_3CR1, and Nrp-1, with scRNA-seq revealing global transcriptional
387 differences that identify them as a discrete subpopulation.
388
389 The persistence of *T. gondii*-induced ILC1s after clearance of infection is reminiscent of classical immune
390 memory and suggests that ex-NK cells play a role beyond what has been attributed to NK cells and ILC1s
391 in *T. gondii* infection thus far. One possibility is that *T. gondii*-induced ILC1s are an inflammatory
392 subpopulation, such as the inflammatory ILC2s that gain circulatory capacity in response to activation by
393 cytokines or infection (Huang et al., 2018). These inflammatory ILC2s can be distinguished from tissue-
394 resident ILC2s based on their increased expression of KLRG1 and S1P receptors, features that are also
395 characteristic of *T. gondii*-induced ILC1s, but not steady-state tissue-resident NK cells. Most *T. gondii*-
396 induced ILC1s express CX_3CR1, which has previously been shown to regulate NK cell recruitment into
397 the circulation (Ponzetta et al., 2013, Sciume et al., 2011). Another possibility is that ex-NK cells may

provide a protective role in subsequent *T. gondii* infections, as shown previously (Denkers et al., 1993), although this finding remains controversial (Goldszmid et al., 2007). Moreover, we have not been able to show that repeated injection of an avirulent *T. gondii* strain confers NK1.1-dependent protection against subsequent lethal re-challenge. Regardless, we have observed ILC1 expansion following repeated exposure to avirulent *T. gondii* strains, and future studies may illuminate how gaining circulatory capacity affects the functionality of ILC1s and how ex-NK cells contribute to subsequent immune responses to *T. gondii*.

In summary, we found that *T. gondii* infection induced permanent changes to NK cells and ILC1s, including conversion of NK cells into ILC1s. Our studies indicate that the current system of ILC classification, based on their phenotype and development under steady state conditions, may not apply following inflammation. Rather, plasticity may give rise to populations that resemble one another at first glance, but actually represent the convergence of multiple developmental paths to form interrelated populations.

Materials and Methods

Mice

Eomes$^{f/f}$, *Tbx21*$^{-/-}$, and *Stat4*$^{-/-}$ were purchased from The Jackson Laboratory. C57BL/6, CD45.1^{+}, and BALB/c mice were purchased from Charles River. *Ncr1*^{iCre} mice were a kind gift from Eric Vivier. *Zeb2*-GFP mice were a generous gift from Kenneth Murphy (Wu et al., 2016). Eomes-GFP mice were graciously provided by Thierry Walzer (Daussy et al., 2014). *Ncr1*^{iCre} were bred to *Eomes*$^{f/f}$ mice to generate *Eomes* cKO mice and Cre-negative littermate controls. *Rag2*$^{-/-}$ were bred to *Il2rg*$^{-/-}$ to generate *Rag2*$^{-/-}$ *Il2rg*$^{-/-}$ mice. Age and sex-matched animals were used in all experiments. Mice were infected at 6-12 wk of age. All protocols were approved by the Institutional Animal Care and Uses Committee (Washington University School of Medicine, St. Louis, MO) under animal protocol number 20160002.

424

425 **Parasites**

426 PRU-FLuc-GFP Type II strain of *T. gondii* was a generous gift from John C. Boothroyd and used in all
427 infections unless otherwise specified. PruΔku80ΔhxΔgra4::HX/mCherry and the wildtype parental strain
428 PruΔku80Δhx were previously described (Jones et al., 2017). The attenuated *Cps1-1* mutant on the type I
429 RH background was described previously (Fox and Bzik, 2002).

430

431 All *T. gondii* strains used in this study were maintained in human foreskin fibroblast (HFF) monolayers
432 grown in D-10 medium (Dulbecco's modified Eagle medium, 10% fetal bovine serum (FBS), 2 mM
433 glutamine, 10 mM HEPES pH 7.5, 20 μg/mL gentamicin), maintained at 37 °C with 5% CO_2. The *Cps1-1*
434 mutant was grown as described above but supplemented with 200 μM uracil (Sigma). Mature parasites
435 were lysed from host cells by vigorous pipetting and egressed parasites were filtered through 3 μm
436 polycarbonate membranes and resuspended in HHE medium (Hanks' balanced salt solution, 10 mM
437 HEPES, 0.1 mM EGTA). Cell cultures were determined to be mycoplasma-negative using the e-Myco
438 plus kit (Intron Biotechnology).

439

440 **Infection**

441 Mice were injected intraperitoneally (i.p.) with 200 PRU-FLuc-GFP, PruΔku80Δhx, or
442 PruΔku80ΔhxΔgra4::HX/mCherry tachyzoites that were propagated in culture as described above. In
443 indicated experiments, mice were treated with 0.5 g/L sulfadiazine in drinking water to suppress parasite
444 growth. To generate non-persistent infections, $1x10^5$ *Cps1-1* tachyzoites were injected 3 times, 2 wk
445 apart.

446

447 **Luciferase Imaging**

448 Mice were injected i.p. with 150 mg D-luciferin (Gold Biotechnology) per kg body weight, incubated for 10
449 min, then anesthetized with continuous isoflurane anesthesia at a flow rate of 1 L/min. Images were
450 captured using an IVIS Spectrum In Vivo Imaging System (Perkin Elmer). Luminescence was quantitated
451 using Living Image software (Perkin Elmer). NK1.1-depleted mice were injected i.p. with 100 μg of α-
452 NK1.1, 3 d and 1 d prior to infection. Purified α-NK1.1 antibody was generated at the Rheumatic
453 Diseases Core Center Protein Purification and Production Facility using the PK136 hybridoma (ATCC).

454

455 **Cell Isolation**

456 Spleens were mashed through a 70 μm cell strainer and treated with Tris-NH_4Cl to lyse red blood cells.
457 Livers were mashed through a 70 μm cell strainer, resuspended in isotonic 38.5% Percoll (Sigma-
458 Aldrich), centrifugated at 325 x g for 20 min, and treated with Tris-NH_4Cl. Peritoneal cells were isolated by
459 lavage of the peritoneal cavity with PBS. Bone marrow was flushed from femurs and tibias, mashed
460 through a 70 μm cell strainer, and treated with Tris-NH_4Cl. Lymph nodes were mashed through a 70 μm
461 cell strainer. Brains were mashed through a 70 μm cell strainer, resuspended in 38.5% isotonic Percoll,
462 and centrifugated at 325 x g for 20 min. Lungs were perfused with PBS, minced, digested in RPMI-1640
463 containing 2% FBS, 1 mg/mL Collagenase Type IV (Sigma-Aldrich), and 0.2 mg/mL DNase (Sigma-
464 Aldrich), mashed through a 70 μm cell strainer, resuspended in 38.5% isotonic Percoll, and centrifugated
465 at 325 x g for 20 min. Uterus and salivary gland were minced, digested in RPMI-1640 containing 0.17
466 mg/mL Liberase TL (Sigma-Aldrich) and 0.1 mg/mL DNase (Roche), mashed through a 70 μm cell
467 strainer, resuspended in 38.5% isotonic Percoll, and centrifugated at 325 x g for 20 min.

468

469 **Flow Cytometry and Cell Sorting**

470 Cells were stained with Fixable Viability Dye and F_c receptors were blocked with 2.4G2 hybridoma
471 (ATCC) culture supernatants prior to staining in PBS containing 2% FBS and 2.5 mM EDTA on ice. Data

was acquired using a FACSCanto instrument (BD Biosciences) or FACSAria instrument (BD Biosciences) using FACSDiva software (BD Biosciences). Data was analyzed with Flowjo v10 (Treestar).

For cell sorting, splenocytes were enriched for NK1.1$^+$ NKp46$^+$ cells by negative selection. Splenocytes were incubated with 0.2 μg/mL biotin anti-mouse CD4, 0.2 μg/mL biotin anti-mouse CD8, and 1 μg/mL biotin anti-mouse CD19. One hundred μL of EasySep Mouse Streptavidin Rapidspheres (BD Biosciences) were added per 1x10^8 splenocytes. Cells were placed in an EasySep magnet (BD Biosciences) and enriched cells were poured off and subjected to extracellular staining. Sorting was performed using a FACSAria instrument (BD Biosciences) using FACSDiva software (BD Biosciences). NK cells were identified as CD3$^-$ CD19$^-$ NK1.1$^+$ NKp46$^+$ Eomes-GFP$^+$ CD49a$^-$ and *T. gondii*-induced ILC1s were identified as CD3$^-$ CD19$^-$ NK1.1$^+$ NKp46$^+$ Eomes-GFP$^-$ CD49a$^+$.

Stimulations and Intracellular Staining

Following extracellular staining, cells were fixed with FoxP3/Transcription Factor Staining Buffer Set for 30 min at room temperature and washed with 1x Permeabilization buffer (eBiosciences). Transcription factor antibodies were diluted in 1x FoxP3 permeabilization buffer and cells were incubated for 30 min at room temperature.

To assess Eomes downregulation after culture in IL-12, 5x10^6 splenocytes were cultured in R-10 medium (RPMI-1640 medium containing 10% FBS, 2 mM glutamine, 100 U/mL penicillin, and 100 μg/mL streptomycin) with 300 IU/mL IL-2 with 20 ng/mL IL-12 (Pepro Tech). Unstimulated control wells contained only 300 IU/mL IL-2.

For detection of IFNγ production, $5x10^6$ splenocytes were cultured for 5 h in R-10, with the addition of 20 ng/mL IL-12, 20 ng/mL IL-12 + 5 ng/mL IL-18, or 0.5 μg/mL PMA + 4 μg/mL Ionomycin. Brefeldin A was added after 1 h.

Generation of Bone Marrow Chimeras

Donor bone marrow was harvested by flushing femurs and tibias and mashing through a 70 μm cell strainer. Cells were mixed in a 1:1 ratio with $CD45.1^+$ bone marrow, and intravenously injected into irradiated mice. Recipient mice were lethally irradiated (900 rad) and reconstituted with a 1:1 ratio of $CD45.1^+$ bone marrow cells and $CD45.2^+$ *Eomes* cKO, $Eomes^{f/f}$, $Tbx21^{-/-}$, or $Stat4^{-/-}$ bone marrow cells (Kaplan et al., 1996, Zhu et al., 2010, Finotto et al., 2002). Mice were maintained on sulfamethoxazole/trimethoprim oral suspension added to the drinking water for 2 wk after reconstitution and used for experiments 6-8 wk after reconstitution. To prevent chimeric mice from succumbing to acute *T. gondii* infection, bone marrow chimeras were treated with 0.5 g/L sulfadiazine in drinking water beginning 10 d.p.i. and maintained on sulfadiazine until the end of the experiment.

Single-Cell RNA-Seq

Sorted cells were subjected to droplet-based 3' end massively parallel single-cell RNA sequencing using Chromium Single Cell 3' Reagent Kits as per manufacturer's instructions (10x Genomics). The libraries were sequenced using a HiSeq3000 instrument (Illumina).

Sample demultiplexing, barcode processing, and single-cell 3' counting was performed using the Cell Ranger Single-Cell Software Suite (10x Genomics). Cellranger count was used to align samples to the mm10 reference genome, quantify reads, and filter reads with a quality score below 30.

519 The Seurat package in R was used for subsequent analysis (Butler et al., 2018). Genes expressed in
520 fewer than 3 cells and cells that expressed less than 400 or greater than 3500 genes were removed for
521 downstream analysis. Data was normalized using a scaling factor of 10,000s and nUMI was regressed
522 with a negative binomial model. Principal component analysis was performed using the top 3000 most
523 variable genes and t-SNE analysis was performed with the top 40 PCAs. Clustering was performed using
524 a resolution of 0.8. For heatmaps, the mean expression by all cells within the cluster was used.

525

526 **RNA Sequencing**

527 RNA was isolated from $5x10^4$ sorted cells using Trizol. Libraries were prepared using the Clontech
528 SMARTer Kit. Sequencing was performed using 1x50 single-end reads with a HiSeq3000 instrument
529 (Illumina). Reads were quantified using kallisto and differential expression was assessed using the
530 DESeq2 package in R (Bray et al., 2016, Love et al., 2014). Using a log2FC cutoff of 1 and an FDR
531 threshold of 0.1, we identified 657 differentially expressed (DE) genes between the NK cells from
532 uninfected and d35-infected mice, 2288 DE genes between NK cells from infected mice and *T. gondii*-
533 induced ILC1s, and 1685 DE genes between NK cells from uninfected mice and *T. gondii*-induced ILC1s.
534 Variance-stabilized transform values were used for subsequent analysis. All plots were generated in R
535 using the ggplot2, pheatmap, and hclust packages. GSEA was performed using the GSEA Preranked
536 module in GenePattern (Subramanian et al., 2005, Mootha et al., 2003, Reich et al., 2006).

537

538 **ATAC-seq**

539 Samples were prepared as previously described (Buenrostro et al., 2015), then purified with MinElute
540 spin columns (Qiagen). DNA fragments were amplified using Nextera index adapters as per
541 manufacturer's instructions (Illumina). Libraries were purified with AMPure XP beads (Beckman Coulter).
542 Three libraries were pooled and sequenced with 2x50 paired end reads using a HiSeq3000 instrument
543 (Illumina).

544

Sequences were aligned to the mm10 reference genome using Bowtie2 (Langmead and Salzberg, 2012). Reads with a quality score below 30 were removed with Samtools (Li et al., 2009) and duplicate reads were filtered with PicardTools (Broad Institute). Peaks were called using MACS2 (Zhang et al., 2008) with an FDR cutoff of 0.05. Narrowpeak files generated from MACS2 were converted to Bigwig files with deepTools (Ramirez et al., 2014), and visualized using the UCSC genome browser. Differential peaks were identified using Homer (Heinz et al., 2010) and heatmaps of differentially accessible regions were generated with deepTools. Transcription factor binding motifs were identified *de novo* with Homer.

Across all samples, we identified 71,504 peaks. We further analyzed 9,640 discrete peaks that displayed two-fold changes between at least two groups. Between NK cells from control and infected mice, there were 1,809 differential peaks (1445 were larger in the NK cells from infected mice and 364 were larger in NK cells from uninfected mice), between NK cells from infected mice and *T. gondii*-induced ILC1s, there were 6,710 differential peaks (4572 were larger in the cNK cells and 2,138 were larger in *T. gondii*-induced ILC1s), and between NK cells from uninfected mice and *T. gondii*-induced ILC1s, there were 5,938 differential peaks (3065 were larger in the uninfected NK cells and 2,973 were larger in *T. gondii*-induced ILC1s).

Statistical Analysis

Prism (GraphPad) was used for statistical analysis. Student's t-test was used for comparison of 2 groups and 2-way ANOVA with Bonferroni correction was used in analyses involving multiple comparisons. P-values are shown in figures and figure legends. In all graphs, points represent biological replicates, bar position represents the mean, and error bars represent + s.e.m.

Data Availability

The sequencing data in this publication are available on GEO. The RNA-seq and ATAC-seq data are accessible under the accession number GSE124313. The scRNA-seq data are available under accession number GSE124577.

Acknowledgements

This work was supported by NIH grants F30DK108472 (E.P.), AI128845 (W.M.Y.), AI120606 (E.M.O), AI134035 (E.M.O., M.C.), AI11852 (E.M.O.), and CA188286 (E.M.O.). We thank members of the Yokoyama Lab, Ilija Brizic, Stipan Jonjic, and Victor Cortez for helpful discussions, Jennifer Barks and Reeha Savari Dhason for HFF cells, Nathaniel Jones, Sumit Kumar, Josh Radke, and Kevin Brown for *T. gondii* strains, Suzanne Hickerson for technical assistance, and Lacey Feigl, Lorraine Schwartz, and Shirley McTigue for administrative assistance.

We thank the Genome Technology Access Center in the Department of Genetics at Washington University School of Medicine for help with genomic analysis. The Center is partially supported by NCI Cancer Center Support Grant #P30 CA91842 to the Siteman Cancer Center and by ICTS/CTSA Grant# UL1 TR000448 from the National Center for Research Resources (NCRR), a component of the National Institutes of Health (NIH), and NIH Roadmap for Medical Research. This publication is solely the responsibility of the authors and does not necessarily represent the official view of NCRR or NIH. We also thank the McDonnell Genome Institute, especially Catrina Fronick, Robert Fulton, and Amy Ly, for assistance and advisement regarding genomic analysis.

Competing Interests

The authors declare no competing interests.

References

BOSCH-DRIESSEN, L. H., PLAISIER, M. B., STILMA, J. S., VAN DER LELIJ, A. & ROTHOVA, A. 2002. Reactivations of ocular toxoplasmosis after cataract extraction. *Ophthalmology,* 109**,** 41-5.

BRAY, N. L., PIMENTEL, H., MELSTED, P. & PACHTER, L. 2016. Near-optimal probabilistic RNA-seq quantification. *Nat Biotechnol,* 34**,** 525-7.

BUENROSTRO, J. D., WU, B., CHANG, H. Y. & GREENLEAF, W. J. 2015. ATAC-seq: A Method for Assaying Chromatin Accessibility Genome-Wide. *Curr Protoc Mol Biol,* 109**,** 21 29 1-9.

BUTLER, A., HOFFMAN, P., SMIBERT, P., PAPALEXI, E. & SATIJA, R. 2018. Integrating single-cell transcriptomic data across different conditions, technologies, and species. *Nat Biotechnol,* 36**,** 411-420.

CAI, G., RADZANOWSKI, T., VILLEGAS, E. N., KASTELEIN, R. & HUNTER, C. A. 2000. Identification of STAT4-dependent and independent mechanisms of resistance to Toxoplasma gondii. *J Immunol,* 165**,** 2619-27.

CONSTANTINIDES, M. G., MCDONALD, B. D., VERHOEF, P. A. & BENDELAC, A. 2014. A committed precursor to innate lymphoid cells. *Nature,* 508**,** 397-401.

COOPER, M. A., ELLIOTT, J. M., KEYEL, P. A., YANG, L., CARRERO, J. A. & YOKOYAMA, W. M. 2009. Cytokine-induced memory-like natural killer cells. *Proc Natl Acad Sci U S A,* 106**,** 1915-9.

CORTEZ, V. S., CERVANTES-BARRAGAN, L., ROBINETTE, M. L., BANDO, J. K., WANG, Y., GEIGER, T. L., GILFILLAN, S., FUCHS, A., VIVIER, E., SUN, J. C., CELLA, M. & COLONNA, M. 2016. Transforming Growth Factor-beta Signaling Guides the Differentiation of Innate Lymphoid Cells in Salivary Glands. *Immunity,* 44**,** 1127-39.

DADI, S., CHHANGAWALA, S., WHITLOCK, B. M., FRANKLIN, R. A., LUO, C. T., OH, S. A., TOURE, A., PRITYKIN, Y., HUSE, M., LESLIE, C. S. & LI, M. O. 2016. Cancer Immunosurveillance by Tissue-Resident Innate Lymphoid Cells and Innate-like T Cells. *Cell,* 164**,** 365-77.

DAUSSY, C., FAURE, F., MAYOL, K., VIEL, S., GASTEIGER, G., CHARRIER, E., BIENVENU, J., HENRY, T., DEBIEN, E., HASAN, U. A., MARVEL, J., YOH, K., TAKAHASHI, S., PRINZ, I., DE BERNARD, S., BUFFAT, L. & WALZER, T. 2014. T-bet and Eomes instruct the development of two distinct natural killer cell lineages in the liver and in the bone marrow. *J Exp Med,* 211**,** 563-77.

DENKERS, E. Y., GAZZINELLI, R. T., MARTIN, D. & SHER, A. 1993. Emergence of NK1.1+ cells as effectors of IFN-gamma dependent immunity to Toxoplasma gondii in MHC class I-deficient mice. *J Exp Med,* 178**,** 1465-72.

EYLES, D. E. & COLEMAN, N. 1955. An evaluation of the curative effects of pyrimethamine and sulfadiazine, alone and in combination, on experimental mouse toxoplasmosis. *Antibiot Chemother (Northfield),* 5**,** 529-39.

FINOTTO, S., NEURATH, M. F., GLICKMAN, J. N., QIN, S., LEHR, H. A., GREEN, F. H., ACKERMAN, K., HALEY, K., GALLE, P. R., SZABO, S. J., DRAZEN, J. M., DE SANCTIS, G. T. & GLIMCHER, L. H. 2002. Development of spontaneous airway changes consistent with human asthma in mice lacking T-bet. *Science,* 295**,** 336-8.

FOX, B. A. & BZIK, D. J. 2002. De novo pyrimidine biosynthesis is required for virulence of Toxoplasma gondii. *Nature,* 415**,** 926-9.

FOX, B. A., FALLA, A., ROMMEREIM, L. M., TOMITA, T., GIGLEY, J. P., MERCIER, C., CESBRON-DELAUW, M. F., WEISS, L. M. & BZIK, D. J. 2011. Type II Toxoplasma gondii KU80 knockout strains enable functional analysis of genes required for cyst development and latent infection. *Eukaryot Cell,* 10**,** 1193-206.

FUCHS, A., VERMI, W., LEE, J. S., LONARDI, S., GILFILLAN, S., NEWBERRY, R. D., CELLA, M. & COLONNA, M. 2013. Intraepithelial type 1 innate lymphoid cells are a unique subset of IL-12- and IL-15-responsive IFN-gamma-producing cells. *Immunity,* 38**,** 769-81.

GAO, Y., SOUZA-FONSECA-GUIMARAES, F., BALD, T., NG, S. S., YOUNG, A., NGIOW, S. F., RAUTELA, J., STRAUBE, J., WADDELL, N., BLAKE, S. J., YAN, J., BARTHOLIN, L., LEE, J. S., VIVIER, E., TAKEDA, K., MESSAOUDENE, M., ZITVOGEL, L., TENG, M. W. L., BELZ, G. T., ENGWERDA, C. R., HUNTINGTON, N. D., NAKAMURA, K., HOLZEL, M. & SMYTH, M. J. 2017. Tumor immunoevasion by the conversion of effector NK cells into type 1 innate lymphoid cells. *Nat Immunol,* 18**,** 1004-1015.

GASTEIGER, G., FAN, X., DIKIY, S., LEE, S. Y. & RUDENSKY, A. Y. 2015. Tissue residency of innate lymphoid cells in lymphoid and nonlymphoid organs. *Science,* 350**,** 981-5.

GAZZINELLI, R. T., HIENY, S., WYNN, T. A., WOLF, S. & SHER, A. 1993. Interleukin 12 is required for the T-lymphocyte-independent induction of interferon gamma by an intracellular parasite and induces resistance in T-cell-deficient hosts. *Proc Natl Acad Sci U S A,* 90**,** 6115-9.

GILL, S., VASEY, A. E., DE SOUZA, A., BAKER, J., SMITH, A. T., KOHRT, H. E., FLOREK, M., GIBBS, K. D., JR., TATE, K., RITCHIE, D. S. & NEGRIN, R. S. 2012. Rapid development of exhaustion

and down-regulation of eomesodermin limit the antitumor activity of adoptively transferred murine natural killer cells. *Blood,* 119**,** 5758-68.

GOLDSZMID, R. S., BAFICA, A., JANKOVIC, D., FENG, C. G., CASPAR, P., WINKLER-PICKETT, R., TRINCHIERI, G. & SHER, A. 2007. TAP-1 indirectly regulates CD4+ T cell priming in Toxoplasma gondii infection by controlling NK cell IFN-gamma production. *J Exp Med,* 204**,** 2591-602.

GOLDSZMID, R. S., CASPAR, P., RIVOLLIER, A., WHITE, S., DZUTSEV, A., HIENY, S., KELSALL, B., TRINCHIERI, G. & SHER, A. 2012. NK cell-derived interferon-gamma orchestrates cellular dynamics and the differentiation of monocytes into dendritic cells at the site of infection. *Immunity,* 36**,** 1047-59.

GORDON, S. M., CHAIX, J., RUPP, L. J., WU, J., MADERA, S., SUN, J. C., LINDSTEN, T. & REINER, S. L. 2012. The transcription factors T-bet and Eomes control key checkpoints of natural killer cell maturation. *Immunity,* 36**,** 55-67.

HARMS PRITCHARD, G., HALL, A. O., CHRISTIAN, D. A., WAGAGE, S., FANG, Q., MUALLEM, G., JOHN, B., GLATMAN ZARETSKY, A., DUNN, W. G., PERRIGOUE, J., REINER, S. L. & HUNTER, C. A. 2015. Diverse roles for T-bet in the effector responses required for resistance to infection. *J Immunol,* 194**,** 1131-40.

HEINZ, S., BENNER, C., SPANN, N., BERTOLINO, E., LIN, Y. C., LASLO, P., CHENG, J. X., MURRE, C., SINGH, H. & GLASS, C. K. 2010. Simple combinations of lineage-determining transcription factors prime cis-regulatory elements required for macrophage and B cell identities. *Mol Cell,* 38**,** 576-89.

HUANG, Y., MAO, K., CHEN, X., SUN, M. A., KAWABE, T., LI, W., USHER, N., ZHU, J., URBAN, J. F., JR., PAUL, W. E. & GERMAIN, R. N. 2018. S1P-dependent interorgan trafficking of group 2 innate lymphoid cells supports host defense. *Science,* 359**,** 114-119.

HUNTER, C. A., SUBAUSTE, C. S., VAN CLEAVE, V. H. & REMINGTON, J. S. 1994. Production of gamma interferon by natural killer cells from Toxoplasma gondii-infected SCID mice: regulation by interleukin-10, interleukin-12, and tumor necrosis factor alpha. *Infect Immun,* 62**,** 2818-24.

JONES, N. G., WANG, Q. & SIBLEY, L. D. 2017. Secreted protein kinases regulate cyst burden during chronic toxoplasmosis. *Cell Microbiol,* 19.

KAPLAN, M. H., SUN, Y. L., HOEY, T. & GRUSBY, M. J. 1996. Impaired IL-12 responses and enhanced development of Th2 cells in Stat4-deficient mice. *Nature,* 382**,** 174-7.

KLOSE, C. S. N., FLACH, M., MOHLE, L., ROGELL, L., HOYLER, T., EBERT, K., FABIUNKE, C., PFEIFER, D., SEXL, V., FONSECA-PEREIRA, D., DOMINGUES, R. G., VEIGA-FERNANDES, H., ARNOLD, S. J., BUSSLINGER, M., DUNAY, I. R., TANRIVER, Y. & DIEFENBACH, A. 2014. Differentiation of type 1 ILCs from a common progenitor to all helper-like innate lymphoid cell lineages. *Cell,* 157**,** 340-356.

LANGMEAD, B. & SALZBERG, S. L. 2012. Fast gapped-read alignment with Bowtie 2. *Nat Methods,* 9**,** 357-9.

LAU, C. M., ADAMS, N. M., GEARY, C. D., WEIZMAN, O. E., RAPP, M., PRITYKIN, Y., LESLIE, C. S. & SUN, J. C. 2018. Epigenetic control of innate and adaptive immune memory. *Nat Immunol,* 19**,** 963-972.

LI, H., HANDSAKER, B., WYSOKER, A., FENNELL, T., RUAN, J., HOMER, N., MARTH, G., ABECASIS, G., DURBIN, R. & GENOME PROJECT DATA PROCESSING, S. 2009. The Sequence Alignment/Map format and SAMtools. *Bioinformatics,* 25**,** 2078-9.

LOVE, M. I., HUBER, W. & ANDERS, S. 2014. Moderated estimation of fold change and dispersion for RNA-seq data with DESeq2. *Genome Biol,* 15**,** 550.

MONTOYA, J. G. & LIESENFELD, O. 2004. Toxoplasmosis. *Lancet,* 363**,** 1965-76.

MOOTHA, V. K., LINDGREN, C. M., ERIKSSON, K. F., SUBRAMANIAN, A., SIHAG, S., LEHAR, J., PUIGSERVER, P., CARLSSON, E., RIDDERSTRALE, M., LAURILA, E., HOUSTIS, N., DALY, M. J., PATTERSON, N., MESIROV, J. P., GOLUB, T. R., TAMAYO, P., SPIEGELMAN, B., LANDER, E. S., HIRSCHHORN, J. N., ALTSHULER, D. & GROOP, L. C. 2003. PGC-1alpha-responsive genes involved in oxidative phosphorylation are coordinately downregulated in human diabetes. *Nat Genet,* 34**,** 267-73.

PENG, H., JIANG, X., CHEN, Y., SOJKA, D. K., WEI, H., GAO, X., SUN, R., YOKOYAMA, W. M. & TIAN, Z. 2013. Liver-resident NK cells confer adaptive immunity in skin-contact inflammation. *J Clin Invest,* 123**,** 1444-56.

PIKOVSKAYA, O., CHAIX, J., ROTHMAN, N. J., COLLINS, A., CHEN, Y. H., SCIPIONI, A. M., VIVIER, E. & REINER, S. L. 2016. Cutting Edge: Eomesodermin Is Sufficient To Direct Type 1 Innate Lymphocyte Development into the Conventional NK Lineage. *J Immunol,* 196**,** 1449-54.

PONZETTA, A., SCIUME, G., BENIGNI, G., ANTONANGELI, F., MORRONE, S., SANTONI, A. & BERNARDINI, G. 2013. CX3CR1 regulates the maintenance of KLRG1+ NK cells into the bone marrow by promoting their entry into circulation. *J Immunol,* 191**,** 5684-94.

RAMIREZ, F., DUNDAR, F., DIEHL, S., GRUNING, B. A. & MANKE, T. 2014. deepTools: a flexible platform for exploring deep-sequencing data. *Nucleic Acids Res,* 42**,** W187-91.

REICH, M., LIEFELD, T., GOULD, J., LERNER, J., TAMAYO, P. & MESIROV, J. P. 2006. GenePattern 2.0. *Nat Genet,* 38**,** 500-1.

ROBINETTE, M. L., FUCHS, A., CORTEZ, V. S., LEE, J. S., WANG, Y., DURUM, S. K., GILFILLAN, S., COLONNA, M. & IMMUNOLOGICAL GENOME, C. 2015. Transcriptional programs define molecular characteristics of innate lymphoid cell classes and subsets. *Nat Immunol,* 16**,** 306-17.

ROMEE, R., SCHNEIDER, S. E., LEONG, J. W., CHASE, J. M., KEPPEL, C. R., SULLIVAN, R. P., COOPER, M. A. & FEHNIGER, T. A. 2012. Cytokine activation induces human memory-like NK cells. *Blood,* 120**,** 4751-60.

ROSMARAKI, E. E., DOUAGI, I., ROTH, C., COLUCCI, F., CUMANO, A. & DI SANTO, J. P. 2001. Identification of committed NK cell progenitors in adult murine bone marrow. *Eur J Immunol,* 31**,** 1900-9.

SCIUME, G., DE ANGELIS, G., BENIGNI, G., PONZETTA, A., MORRONE, S., SANTONI, A. & BERNARDINI, G. 2011. CX3CR1 expression defines 2 KLRG1+ mouse NK-cell subsets with distinct functional properties and positioning in the bone marrow. *Blood,* 117**,** 4467-75.

SHIH, H. Y., SCIUME, G., MIKAMI, Y., GUO, L., SUN, H. W., BROOKS, S. R., URBAN, J. F., JR., DAVIS, F. P., KANNO, Y. & O'SHEA, J. J. 2016. Developmental Acquisition of Regulomes Underlies Innate Lymphoid Cell Functionality. *Cell,* 165**,** 1120-1133.

SILVER, J. S. & HUMBLES, A. A. 2017. NK cells join the plasticity party. *Nat Immunol,* 18**,** 959-960.

SOJKA, D. K., PLOUGASTEL-DOUGLAS, B., YANG, L., PAK-WITTEL, M. A., ARTYOMOV, M. N., IVANOVA, Y., ZHONG, C., CHASE, J. M., ROTHMAN, P. B., YU, J., RILEY, J. K., ZHU, J., TIAN, Z. & YOKOYAMA, W. M. 2014a. Tissue-resident natural killer (NK) cells are cell lineages distinct from thymic and conventional splenic NK cells. *Elife,* 3**,** e01659.

SOJKA, D. K., TIAN, Z. & YOKOYAMA, W. M. 2014b. Tissue-resident natural killer cells and their potential diversity. *Semin Immunol,* 26**,** 127-31.

SPITS, H., ARTIS, D., COLONNA, M., DIEFENBACH, A., DI SANTO, J. P., EBERL, G., KOYASU, S., LOCKSLEY, R. M., MCKENZIE, A. N., MEBIUS, R. E., POWRIE, F. & VIVIER, E. 2013. Innate lymphoid cells--a proposal for uniform nomenclature. *Nat Rev Immunol,* 13**,** 145-9.

SPITS, H. & CUPEDO, T. 2012. Innate lymphoid cells: emerging insights in development, lineage relationships, and function. *Annu Rev Immunol,* 30**,** 647-75.

SUBRAMANIAN, A., TAMAYO, P., MOOTHA, V. K., MUKHERJEE, S., EBERT, B. L., GILLETTE, M. A., PAULOVICH, A., POMEROY, S. L., GOLUB, T. R., LANDER, E. S. & MESIROV, J. P. 2005. Gene set enrichment analysis: a knowledge-based approach for interpreting genome-wide expression profiles. *Proc Natl Acad Sci U S A,* 102**,** 15545-50.

SUN, J. C., MADERA, S., BEZMAN, N. A., BEILKE, J. N., KAPLAN, M. H. & LANIER, L. L. 2012. Proinflammatory cytokine signaling required for the generation of natural killer cell memory. *J Exp Med,* 209**,** 947-54.

SUZUKI, Y., ORELLANA, M. A., WONG, S. Y., CONLEY, F. K. & REMINGTON, J. S. 1993. Susceptibility to chronic infection with Toxoplasma gondii does not correlate with susceptibility to acute infection in mice. *Infect Immun,* 61**,** 2284-8.

TOWNSEND, M. J., WEINMANN, A. S., MATSUDA, J. L., SALOMON, R., FARNHAM, P. J., BIRON, C. A., GAPIN, L. & GLIMCHER, L. H. 2004. T-bet regulates the terminal maturation and homeostasis of NK and Valpha14i NKT cells. *Immunity,* 20**,** 477-94.

VIVIER, E., ARTIS, D., COLONNA, M., DIEFENBACH, A., DI SANTO, J. P., EBERL, G., KOYASU, S., LOCKSLEY, R. M., MCKENZIE, A. N. J., MEBIUS, R. E., POWRIE, F. & SPITS, H. 2018. Innate Lymphoid Cells: 10 Years On. *Cell,* 174**,** 1054-1066.

WEIZMAN, O. E., ADAMS, N. M., SCHUSTER, I. S., KRISHNA, C., PRITYKIN, Y., LAU, C., DEGLI-ESPOSTI, M. A., LESLIE, C. S., SUN, J. C. & O'SULLIVAN, T. E. 2017. ILC1 Confer Early Host Protection at Initial Sites of Viral Infection. *Cell,* 171**,** 795-808 e12.

WU, X., BRISENO, C. G., GRAJALES-REYES, G. E., HALDAR, M., IWATA, A., KRETZER, N. M., KC, W., TUSSIWAND, R., HIGASHI, Y., MURPHY, T. L. & MURPHY, K. M. 2016. Transcription factor Zeb2 regulates commitment to plasmacytoid dendritic cell and monocyte fate. *Proc Natl Acad Sci U S A,* 113**,** 14775-14780.

YANG, Q., LI, F., HARLY, C., XING, S., YE, L., XIA, X., WANG, H., WANG, X., YU, S., ZHOU, X., CAM, M., XUE, H. H. & BHANDOOLA, A. 2015. TCF-1 upregulation identifies early innate lymphoid progenitors in the bone marrow. *Nat Immunol,* 16**,** 1044-50.

YAROVINSKY, F. 2014. Innate immunity to Toxoplasma gondii infection. *Nat Rev Immunol,* 14**,** 109-21.

YOKOYAMA, W. M. 2013. *In:* PAUL, W. E. (ed.) *Natural Killer Cells (7th Edition).* Lippincott Williams & Wilkins.

ZHANG, Y., LIU, T., MEYER, C. A., EECKHOUTE, J., JOHNSON, D. S., BERNSTEIN, B. E., NUSBAUM, C., MYERS, R. M., BROWN, M., LI, W. & LIU, X. S. 2008. Model-based analysis of ChIP-Seq (MACS). *Genome Biol,* 9**,** R137.

ZHU, Y., JU, S., CHEN, E., DAI, S., LI, C., MOREL, P., LIU, L., ZHANG, X. & LU, B. 2010. T-bet and eomesodermin are required for T cell-mediated antitumor immune responses. *J Immunol,* 185**,** 3174-83.

Figure Legends

Fig. 1: *T. gondii* infection results in ILC1 expansion.

a-e, Wild-type mice were infected by i.p. injection of 200 tachyzoites of the Prugniaud (Pru) strain of *T. gondii*. Splenocytes were analyzed at indicated time points p.i. **a,** Representative flow cytometry plots for the analysis of NK cells (Eomes$^+$ CD49a$^-$) and ILC1s (Eomes$^-$ CD49a$^+$), and Ly6C expression by NK cells and ILC1s, at indicated time points p.i., among CD3$^-$ CD19$^-$ cells. **b,c,** Frequency and absolute number of NK cells (**b**) and ILC1s (**c**) from spleens of uninfected mice and mice at indicated time points p.i. Numbers derived from gates indicated in (**a**), $n = 5$ mice. **d,** Frequency of ILC1s that express Ly6C at indicated time points p.i., $n = 5$ mice. **e,** Representative flow cytometry plots for the analysis of NK cells and ILC1s, and their frequency and absolute number 4 mo p.i., $n = 6$ mice (uninfected) or $n = 7$ mice (infected). Mean + s.e.m (**b-e**); one-way ANOVA with Bonferroni correction (**b-d**); unpaired t-test (**e**); $^*p \leq 0.05$, $^{**}p \leq 0.01$, $^{***}p \leq 0.001$, $^{****}p \leq 0.0001$. Data are representative of 5 independent experiments.

Fig. 2: ILC1 expansion persists in the absence of ongoing infection.

a-d, Representative flow cytometry plots for the analysis of NK cells (Eomes$^+$ CD49a$^-$) and ILC1s (Eomes$^-$ CD49a$^+$), and frequency and absolute number of ILC1s in the spleen following (**a**) treatment with sulfadiazine (SDZ) beginning at indicated time points p.i. and maintained on sulfadiazine until 35 d p.i. when they were analyzed, $n = 5$-11 mice; (**b**) injection with $1x10^5$ tachyzoites 3 times, 2 wk apart, and

analyzed 42 d after initial injection, *n* = 4 mice (uninfected) or *n* = 5 mice (*Cps1-1*); (**c**) infection with PruΔku80 (WT) and PruΔku80Δgra4 (Δgra4) *T. gondii* analyzed 35 d.p.i., *n* = 8 mice (WT) or *n* = 10 mice (Δgra4); (**d**) infection of BALB/c mice 35 d.p.i. Mean + s.e.m (**a-d**); one-way ANOVA with Bonferroni correction (**b**); unpaired t-test (**b-d**); *ns* not significant, $*p \leq 0.05$, $**p \leq 0.01$, $***p \leq 0.001$, $****p \leq 0.0001$. Data are representative of 3 independent experiments.

Fig. 3: ILC1s expand throughout the circulation.

a, Representative flow cytometry plots for the analysis of NK cells and ILC1s in the blood and lung of uninfected and d35-infected mice. **b**, Absolute number of ILC1s in the blood and lung of uninfected and d35 infected mice. **c**, Frequency of ILC1s among NK1.1$^+$ NKp46$^+$ cells in indicated organ at 35 d.p.i., *n* = 3-5 mice. **d**, Overview of competitive transfer experiment. At 35 d.p.i., Eomes-GFP$^+$ CD49a$^-$ and Eomes-GFP$^-$ CD49a$^+$ cells were sorted from CD45.2 and CD45.1 x CD45.2 *Eomes*-GFP reporter mice, respectively. Cells were combined in a 1:1 ratio and intravenously injected into *Rag2*$^{-/-}$ *Il2rg*$^{-/-}$ mice. 24 d later, spleens and livers of recipients were assessed for transferred cells. **e**, Representative flow cytometry plots of CD45.1 and CD45.2 expression by transferred cells in the spleen and liver of *Rag2*$^{-/-}$ *Il2rg*$^{-/-}$ mice, and frequency of transferred NK cells (CD45.2$^+$) and ILC1s (CD45.1$^+$ CD45.2$^+$) 24 d post-transfer, as described in (**d**), *n* = 5 mice. **f**, Representative flow cytometry plots of Eomes-GFP and CD49a expression by transferred NK cells and ILC1s in the spleen (top) and liver (bottom) of *Rag2*$^{-/-}$ *Il2rg*$^{-/-}$ mice, and frequency of Eomes$^-$ CD49a$^+$ 24 d post-transfer, as described in (**d**), *n* = 5 mice. **g,** Representative flow cytometry plots for the analysis of NK cells, ILC1s, and Eomes$^+$ CD49a$^+$ cells, and Ly6C expression by NK cells and ILC1s in the liver at indicated time points p.i. **h,i,j,** Frequency and absolute number of NK cells (**h**), Eomes$^+$ CD49a$^+$ cells (**i**), and ILC1s (**j**), in livers of uninfected and d35-infected mice, *n* = 3 mice (uninfected) or *n* = 5 (infected). **k,** Frequency of ILC1s that express Ly6C, and absolute number of Ly6C$^+$ ILC1s and Ly6C$^-$ ILC1s from livers of uninfected and d35-infected mice, *n* = 3 mice (uninfected) or *n* = 5 (infected). Mean + s.e.m. (**b,c,e,f,h-k**); unpaired t-test (**b,f,h-k**); one-way

826 ANOVA with Bonferroni correction (**c, e**); *ns* not significant, *$p \leq 0.05$, **$p \leq 0.01$, ***$p \leq 0.001$, ****$p \leq$
827 0.0001. Data are representative of 3 independent experiments.

828

829 **Fig. 4: *T. gondii*-induced ILC1s are distinct from NK Cells and ILC1s.**
830 **a-d**, Representative flow cytometry plots showing expression of indicated markers by NK cells and ILC1s
831 in uninfected and d35-infected mice, and frequency of each cell population that expresses each marker, *n*
832 = 3-5. **e,f,** Representative flow cytometry plots and frequency of NK cells and ILC1s in uninfected and
833 d35-infected mice after 4 h culture with indicated stimulus that contain intracellular IFNγ (**e**) or TNFα (**f**), *n*
834 = 5. Mean + s.e.m. (**a-f**); one-way ANOVA with Bonferroni correction (**a-f**); *$p \leq 0.05$, **$p \leq 0.01$, ***$p \leq$
835 0.001, ****$p \leq 0.0001$. Data are representative of 3 independent experiments.

836

837 **Fig. 5: *T. gondii* infection induces heterogeneity of NK Cells and ILC1s.**
838 **a**, Representative flow cytometry plots showing Tbet expression by NK cells and ILC1s in uninfected and
839 d35-infected mice, and gMFI of Tbet expression by each population, *n* = 3 mice (uninfected) or *n* = 5 mice
840 (infected). **b**, Representative flow cytometry plots for the analysis of NK cells, ILC1s, and Eomes$^+$ CD49a$^+$
841 cells, among CD45.1-derived (WT) or CD45.2-derived (*Tbx21*$^{-/-}$) cells from spleens and livers of
842 uninfected and d35-infected WT:*Tbx21*$^{-/-}$ bone marrow chimeras, and frequency of Eomes$^+$ CD49a$^+$ cells,
843 *n* = 4 mice (uninfected) or *n* = 7 mice (infected). **c**, Biaxial t-SNE analysis of cells pooled across all
844 samples. Points represent individual cells, colors denote different clusters. **d**, Fraction of cells in C1-C17
845 within each sample. **f**, Heatmap of average expression of select genes that are characteristic of C1-C17.
846 **g**, Expression of indicated genes by cells in each sample. Mean + s.e.m. (**a,b**); one-way ANOVA with
847 Bonferroni correction (**a,b**); *ns* not significant *$P \leq 0.05$, **$p \leq 0.01$, ****$p \leq 0.0001$; data are representative
848 of 3 independent experiments (**a-c**).

849

850 **Fig. 6: NK Cells downregulate Eomes during *T. gondii* infection.**

a, Representative flow cytometry plots for the analysis of ILC1s (CD49a$^+$) or Ly6C$^+$ ILC1s (CD49a$^+$ Ly6C$^+$), and **b**, absolute number of these cells in the spleens of *Eomes*$^{f/f}$ and *Eomes* cKO mice 35 d.p.i., n = 6-9 mice. The increased number of CD49a$^+$ Ly6C$^+$ cells in infected versus uninfected *Eomes*$^{fl/fl}$ mice represent both NK cells and ILC1s whereas in cKO mice, the increased number represents ILC1s only, as indicated by the brackets. **c,** Representative flow cytometry plot showing expression of Ly6C and frequency of ILC1s that express Ly6C, n = 6-9 mice. **d**, Representative flow cytometry plots for the analysis of ILC1 chimerism in the spleens of uninfected and d35-infected WT:*Eomes*$^{f/f}$ and WT:*Eomes* cKO bone marrow chimeras, and frequency of ILC1s that are derived from WT, *Eomes*$^{f/f}$, or *Eomes* cKO bone marrow, n = 4 mice (uninfected) or n = 5 (infected). **e**, Representative flow cytometry plots for the analysis of NK cell and ILC1 chimerism in the spleens of uninfected and d35-infected WT:*Stat4*$^{-/-}$ bone marrow chimeras, and frequency of NK cells and ILC1s that are derived from WT or *Stat4*$^{-/-}$ bone marrow, n = 3 mice. Mean + s.e.m. (**b-d**); one-way ANOVA with Bonferroni correction (**b-d**); *ns* not significant *$p \leq$ 0.05, **$p \leq 0.01$, ****$p \leq 0.0001$. Data are representative of 3 independent experiments.

Fig. 7: Eomes downregulation within NK cells accompanies extensive transcriptional and epigenomic changes.

a, Principal component analysis using top 2000 most variable genes from RNA-seq analysis comparing NK cells from spleens of uninfected and infected mice and Ly6C$^+$ ILC1s from d35-infected mice, n = 3 mice. **b**, Unsupervised hierarchical clustering of samples in (**a**). **c**, Volcano plots showing Log_2(Fold Change) differences versus $-Log_{10}$(False Discovery Rate) for indicated comparisons. Genes exhibiting $Log_2FC > 1$ and FDR < 0.1 are colored. **d**, Heatmaps showing centered DESeq2 variance-stabilized expression values of select genes exhibiting $Log_2FC > 1$ and FDR < 0.1. **e**, Principal component analysis from ATAC-seq analysis comparing NK cells from spleens of uninfected and infected mice and Ly6C$^+$ ILC1s from d35-infected mice, n = 3 mice. **f**, Unsupervised hierarchical clustering of samples in (**e**). **g**, Representative UCSC genome browser tracks showing ATAC-seq peaks in NK cells from uninfected

876 mice, and NK cells and Ly6C$^+$ ILC1s from d35-infected mice, at the *Eomes* locus. Differentially accessible
877 REs are highlighted in blue.

878

879 **Supplementary Fig. 1: α-NK1.1 depletion increases parasite burden and mortality in *T. gondii***
880 **infection.**
881 **a**, Representative luciferase images of undepleted mice and α-NK1.1-depleted mice lying supine, at
882 indicated time points after infection with 200 Pru.Luc *T. gondii* parasites. α-NK1.1-depleted mice were
883 injected with 100 μg of α-NK1.1 i.p. 2 days prior to infection and the day of infection. **b**, Total photon flux
884 measured in undepleted mice and α-NK1.1-depleted mice, at indicated time points after infection, $n = 5$.
885 **c**, Percentage of mice surviving at indicated time points after infection, $n = 10$. Mean + s.e.m. unpaired t-
886 test, $^*p \leq 0.05$ (**b**), Mantel-Cox test, $^*p \leq 0.01$ (**c**). Data are representative of 3 independent experiments.
887

888 **Supplementary Fig. 2: ILC1s expand at additional sites beyond the spleen.**
889 **a**, Representative flow cytometry plots showing Ly6C expression by ILC1s in the blood and lungs of
890 uninfected mice or at 35 d.p.i. **b**, Representative flow cytometry plots for the assessment of NK cells and
891 ILC1s in the indicated organs of uninfected mice or at 35 d.p.i. Data are representative of 3 independent
892 experiments.
893

894 **Supplementary Fig. 3: Ly6C expression distinguishes between ILC1 subpopulations.**
895 **a,b,** Representative flow cytometry plots for the analysis of NK cells from the blood of uninfected mice
896 and at 35 d.p.i. and ILC1s at 35 d.p.i. and frequency of each cell population that expresses indicated
897 markers, $n = 5$. **c,** Representative flow cytometry plots for the analysis of NK cells (Eomes$^+$ CD49a$^-$),
898 Ly6C$^-$ ILC1s (Eomes$^-$ CD49a$^+$ Ly6C$^-$), and Ly6C$^+$ ILC1s (Eomes$^-$ CD49a$^+$ Ly6C$^+$) in the livers of
899 uninfected mice and at 35 d.p.i. **d**, Representative flow cytometry plots and frequency of each cell
900 population that expresses indicated markers, $n = 3$-5. **f,** Representative flow cytometry plots and
901 frequency of each population that produced TNFα after 4 h culture with indicated stimulus, $n = 3$. Mean +

s.e.m. (**a,b,d-f**); one-way ANOVA with Bonferroni correction (**a,b,d-f**); *ns* not significant *$p \leq 0.05$, **$p \leq 0.01$, ****$p \leq 0.0001$. Data are representative of 3 independent experiments.

Supplementary Fig. 4: Single-cell RNA-seq reveals extensive NK cells and ILC1 heterogeneity in the liver.

a, Representative flow cytometry plots for the analysis of NK cell and ILC1 chimerism in the spleens of uninfected and d35-infected WT:*Tbx21*$^{-/-}$ bone marrow chimeras, and frequency of NK cells and ILC1s that are derived from WT or *Tbx21*$^{-/-}$ bone marrow. **b**, Representative flow cytometry plots for the expression of CD27 and CD11b by NK cells from the livers of uninfected and d35-infected mice. **c**, Frequency of indicated cell types in uninfected and d35-infected mice, $n = 3$. **d**, t-SNE plot labeled with putative cluster identities. **e**, Heatmap of average expression of signature ILC1 and NK cell genes by cells in Clusters 1, 3, 10, and 11 (Robinette et al., 2015). **f**, Representative flow cytometry plots showing the expression of CX_3CR1 and CXCR6 by indicated populations. **g**, Expression of Zeb2 by CXCR6$^+$ Ly6C$^+$ ILC1s and CX_3CR1^+ Ly6C$^+$ ILC1s from the liver of d35-infected *Zeb2*-GFP mice, $n = 3$. Mean + s.e.m. (**a,b,g**); one-way ANOVA with Bonferroni correction (**a**); paired t-test (**g**); *$p \leq 0.05$, ****$p \leq 0.0001$. Data are representative of 3 independent experiments (**a,b,c,f,g**).

Supplementary Fig. 5: IL-12 contributes to Eomes downregulation.

a, Representative flow cytometry plots for the quantification of NK1.1$^+$ NKp46$^+$ cells from spleens of uninfected and d35-infected *Eomes*$^{f/f}$ and *Eomes* cKO mice, and absolute number of cells, $n = 6$-9 mice. **b**, Representative flow cytometry plots for the quantification of ILC1s (Eomes$^-$ CD49a$^+$) after culture of splenocytes from uninfected and d35-infected mice in IL-2, or IL-2 + IL-12, and frequency of ILC1s, $n = 3$ mice (uninfected) or $n = 12$ mice (infected). **c**, Representative flow cytometry plots for the assessment of Eomes and CD49a expression of sorted NK cells or ILC1s from uninfected or d35-infected mice after culture in IL-2, or IL-2 + IL-12, and frequency of Eomes$^-$ CD49a$^+$ cells, $n = 3$-7 wells. Mean + s.e.m. (**a-c**);

one-way ANOVA with Bonferroni correction (**a-c**); *ns* not significant, *$p \leq 0.01$, ****$p \leq 0.0001$. Data are representative of 3 independent experiments.

Supplementary Fig. 6: ATAC-seq analysis reveals widespread changes in chromatin accessibility in *T. gondii*-induced ILC1s.

a, Representative flow cytometry plots for sorting NK cells (CD49a$^-$ Ly6C$^-$) and ILC1s (CD49a$^+$ Ly6C$^+$) from the spleens of uninfected and infected mice, and expression of Eomes by each population. **b**, Quantification of regulatory elements with log2FC>1 and FDR<0.05 within indicated genomic regions in pairwise comparison of NK cells from infected mice versus NK cells from uninfected mice (left), *T. gondii*-induced ILC1s and NK cells from infected mice (middle), and *T. gondii*-induced ILC1s and NK cells from uninfected mice (right). **c,** Heatmap of differentially accessible REs, centered on peaks and showing 3 kb upstream and downstream of peak center. **d**, *De novo* transcription factor binding motifs found enriched in Clusters 3 and 5, and p-values for enrichment compared to background regions. **e**, For each gene listed, Log2FC of gene expression from RNA-seq is indicated by position of bottom point. Each differentially accessible RE is depicted as a point, with Log2FC of peak size in *T. gondii*-induced ILC1s relative to NK cells indicated by fill color of each point. **f**, Representative UCSC genome browser tracks showing ATAC-seq peaks in NK cells from uninfected mice, and NK cells and Ly6C$^+$ ILC1s from d35-infected mice, at the *Tbx21* locus. Differentially accessible REs are highlighted in blue.

Figure 1

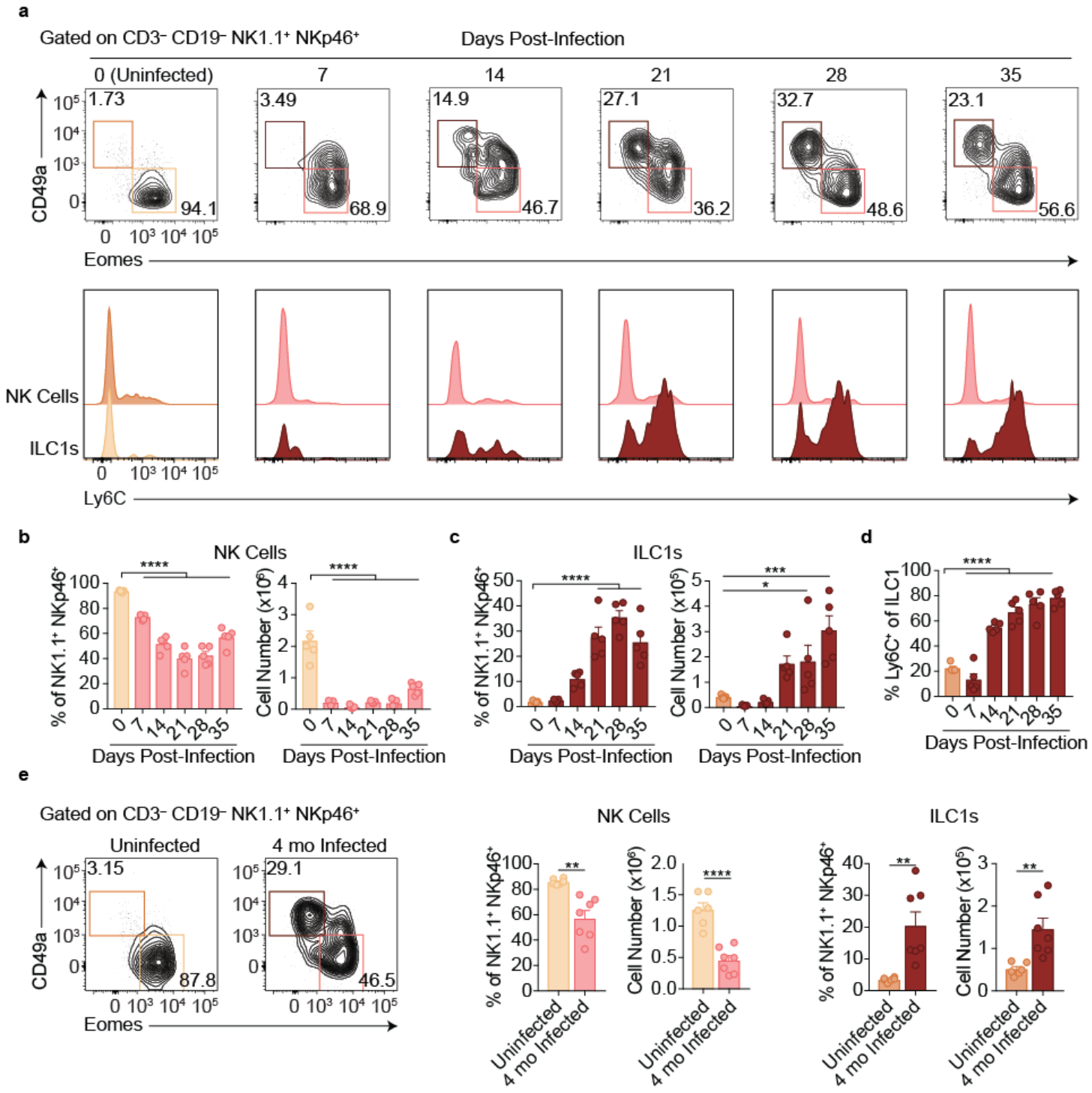
a
Gated on CD3⁻ CD19⁻ NK1.1⁺ NKp46⁺
Days Post-Infection
0 (Uninfected)
7
14
21
28
35
1.73
94.1
3.49
68.9
14.9
46.7
27.1
36.2
32.7
48.6
23.1
56.6
CD49a
Eomes
NK Cells
ILC1s
Ly6C
b
NK Cells
% of NK1.1⁺ NKp46⁺
Cell Number (x10⁶)
Days Post-Infection
c
ILC1s
% of NK1.1⁺ NKp46⁺
Cell Number (x10⁵)
Days Post-Infection
d
% Ly6C⁺ of ILC1
Days Post-Infection
e
Gated on CD3⁻ CD19⁻ NK1.1⁺ NKp46⁺
Uninfected
4 mo Infected
3.15
87.8
29.1
46.5
CD49a
Eomes
NK Cells
ILC1s
% of NK1.1⁺ NKp46⁺
Cell Number (x10⁶)
Cell Number (x10⁵)
Uninfected
4 mo Infected

Figure 2

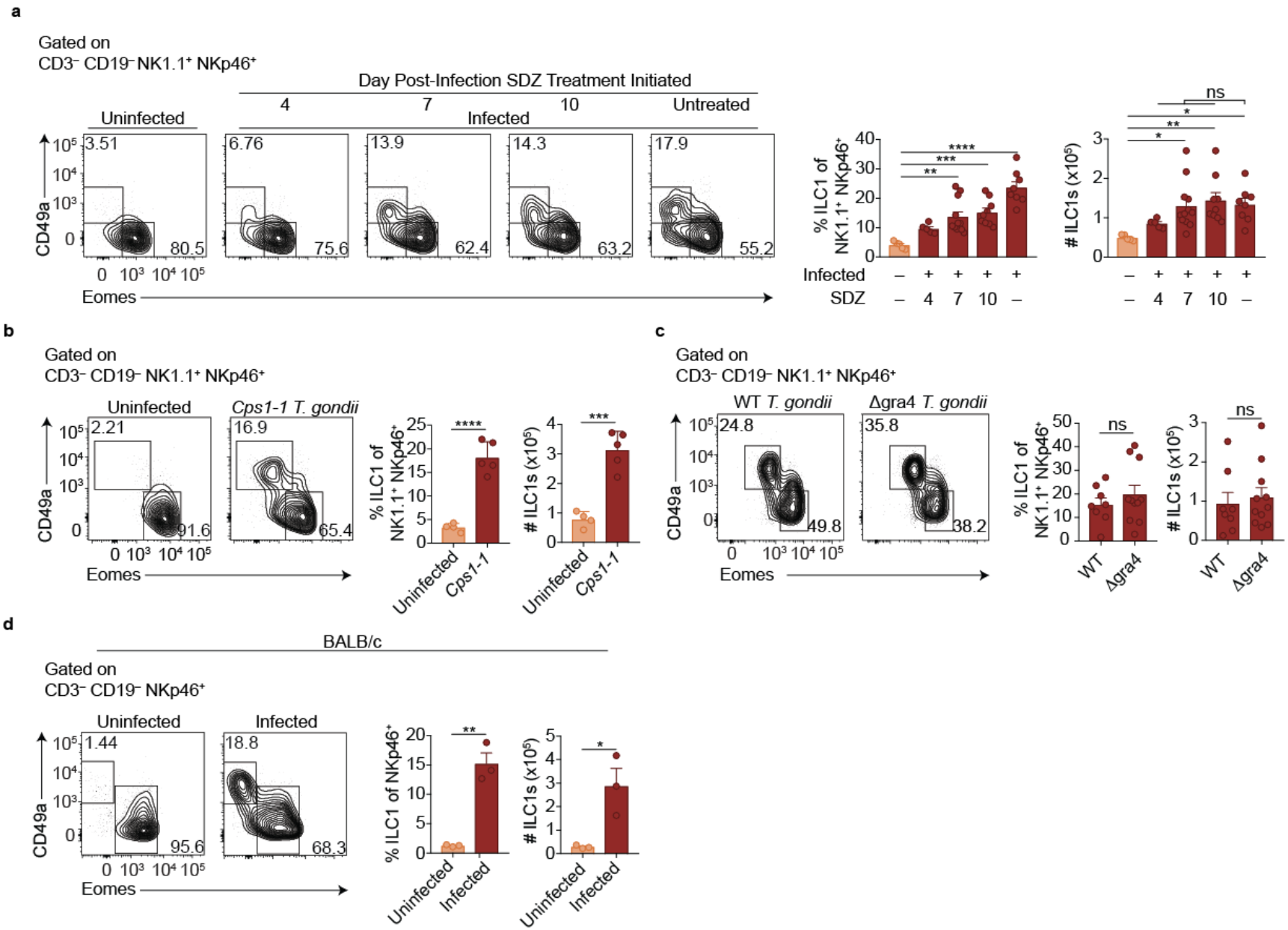
a
Gated on
CD3⁻ CD19⁻ NK1.1⁺ NKp46⁺
Day Post-Infection SDZ Treatment Initiated
Uninfected
4
7
10
Untreated
Infected
CD49a
Eomes
3.51
80.5
6.76
75.6
13.9
62.4
14.3
63.2
17.9
55.2
% ILC1 of NK1.1⁺ NKp46⁺
# ILC1s (x10⁵)
Infected
SDZ
ns
b
Gated on
CD3⁻ CD19⁻ NK1.1⁺ NKp46⁺
Uninfected
Cps1-1 T. gondii
2.21
91.6
16.9
65.4
% ILC1 of NK1.1⁺ NKp46⁺
# ILC1s (x10⁵)
Uninfected
Cps1-1
c
Gated on
CD3⁻ CD19⁻ NK1.1⁺ NKp46⁺
WT T. gondii
Δgra4 T. gondii
24.8
49.8
35.8
38.2
% ILC1 of NK1.1⁺ NKp46⁺
# ILC1s (x10⁵)
WT
Δgra4
d
BALB/c
Gated on
CD3⁻ CD19⁻ NKp46⁺
Uninfected
Infected
1.44
95.6
18.8
68.3
% ILC1 of NKp46⁺
# ILC1s (x10⁵)

Figure 3

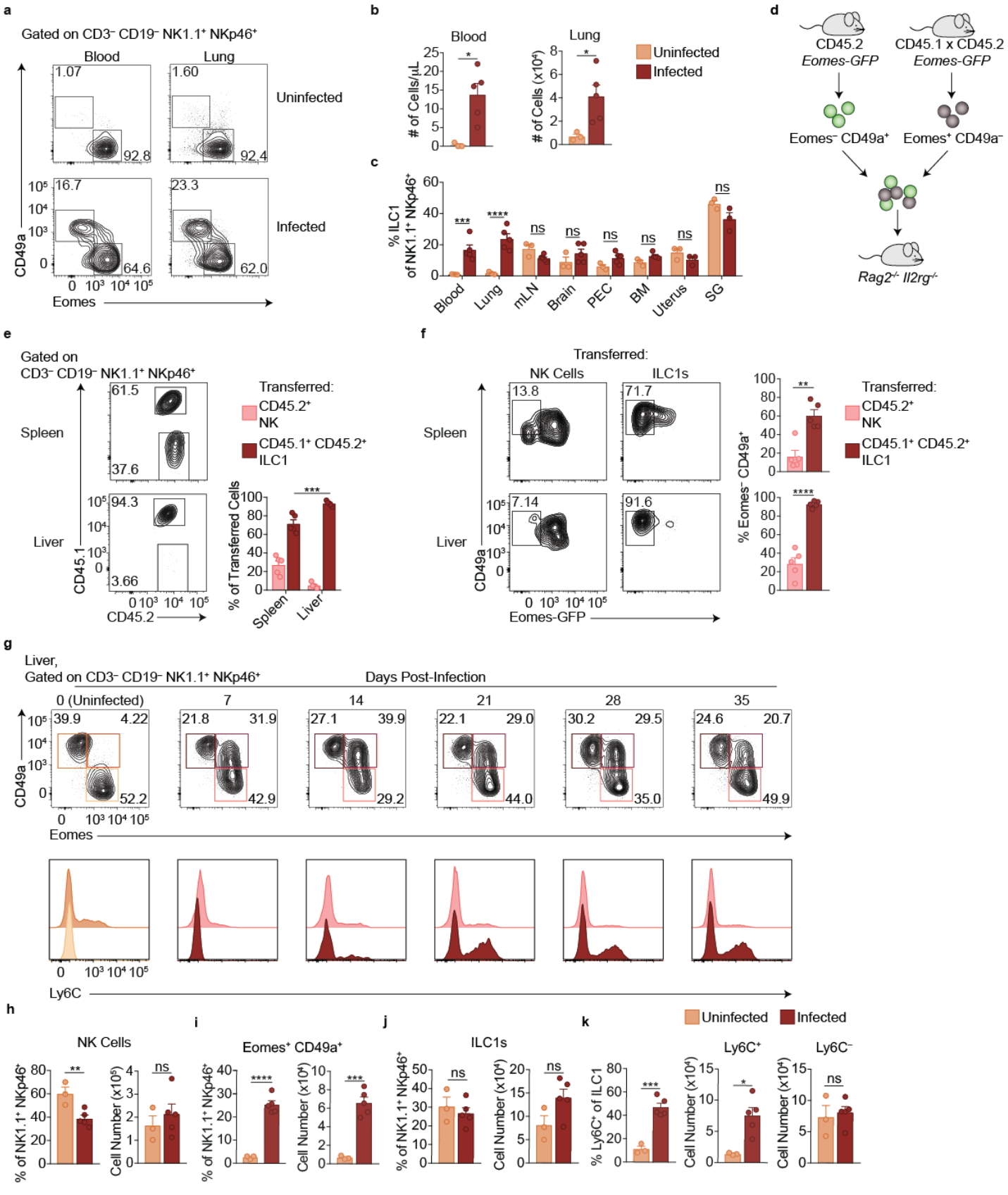
a
Gated on CD3⁻ CD19⁻ NK1.1⁺ NKp46⁺
Blood
Lung
Uninfected
Infected
CD49a
Eomes
b
Blood
Lung
# of Cells/µL
# of Cells (x10⁴)
Uninfected
Infected
c
% ILC1 of NK1.1⁺ NKp46⁺
Blood
Lung
mLN
Brain
PEC
BM
Uterus
SG
d
CD45.2
Eomes-GFP
CD45.1 x CD45.2
Eomes-GFP
Eomes⁻ CD49a⁺
Eomes⁺ CD49a⁻
Rag2⁻/⁻ Il2rg⁻/⁻
e
Gated on
CD3⁻ CD19⁻ NK1.1⁺ NKp46⁺
Spleen
Liver
CD45.1
CD45.2
Transferred:
CD45.2⁺ NK
CD45.1⁺ CD45.2⁺ ILC1
% of Transferred Cells
f
Transferred:
NK Cells
ILC1s
Spleen
Liver
CD49a
Eomes-GFP
% Eomes⁻ CD49a⁺
g
Liver,
Gated on CD3⁻ CD19⁻ NK1.1⁺ NKp46⁺
Days Post-Infection
0 (Uninfected)
7
14
21
28
35
CD49a
Eomes
Ly6C
h
NK Cells
% of NK1.1⁺ NKp46⁺
Cell Number (x10⁵)
i
Eomes⁺ CD49a⁺
% of NK1.1⁺ NKp46⁺
Cell Number (x10⁴)
j
ILC1s
% of NK1.1⁺ NKp46⁺
Cell Number (x10⁴)
k
Uninfected
Infected
% Ly6C⁺ of ILC1
Ly6C⁺
Cell Number (x10⁴)
Ly6C⁻
Cell Number (x10⁴)

Figure 4

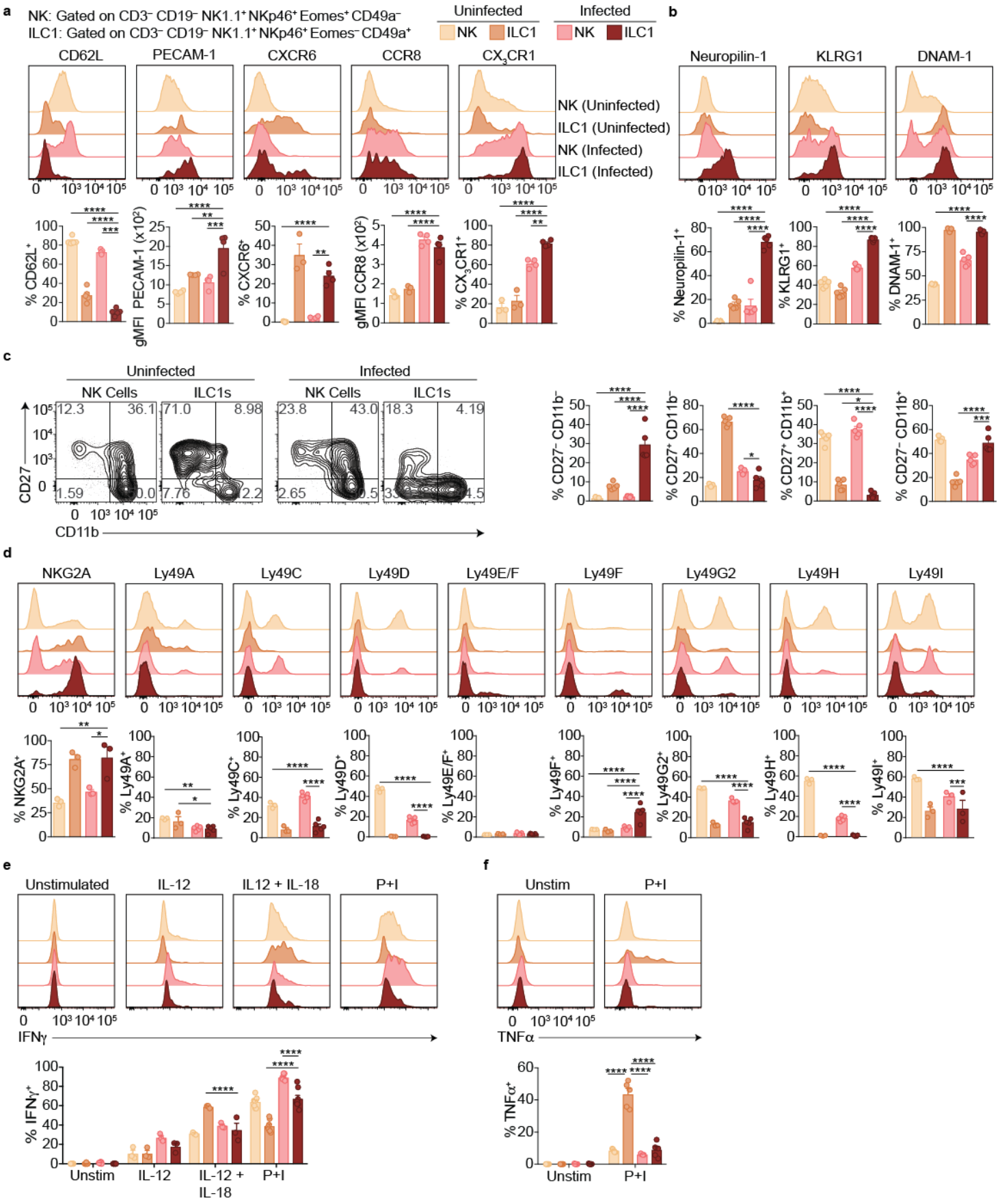
a
NK: Gated on CD3⁻ CD19⁻ NK1.1⁺ NKp46⁺ Eomes⁺ CD49a⁻
ILC1: Gated on CD3⁻ CD19⁻ NK1.1⁺ NKp46⁺ Eomes⁻ CD49a⁺
Uninfected
NK
ILC1
Infected
NK
ILC1
CD62L
PECAM-1
CXCR6
CCR8
CX3CR1
NK (Uninfected)
ILC1 (Uninfected)
NK (Infected)
ILC1 (Infected)
% CD62L+
gMFI PECAM-1 (x10²)
% CXCR6+
gMFI CCR8 (x10²)
% CX3CR1+
b
Neuropilin-1
KLRG1
DNAM-1
% Neuropilin-1+
% KLRG1+
% DNAM-1+
c
Uninfected
Infected
NK Cells
ILC1s
NK Cells
ILC1s
12.3
36.1
71.0
8.98
23.8
43.0
18.3
4.19
1.59
0.0
7.76
2.2
2.65
0.5
CD27
CD11b
% CD27⁻ CD11b⁻
% CD27⁺ CD11b⁻
% CD27⁺ CD11b⁺
% CD27⁻ CD11b⁺
d
NKG2A
Ly49A
Ly49C
Ly49D
Ly49E/F
Ly49F
Ly49G2
Ly49H
Ly49I
% NKG2A+
% Ly49A+
% Ly49C+
% Ly49D+
% Ly49E/F+
% Ly49F+
% Ly49G2+
% Ly49H+
% Ly49I+
e
Unstimulated
IL-12
IL12 + IL-18
P+I
IFNγ
% IFNγ+
Unstim
IL-12
IL-12 + IL-18
P+I
f
Unstim
P+I
TNFα
% TNFα+
Unstim
P+I

Figure 5

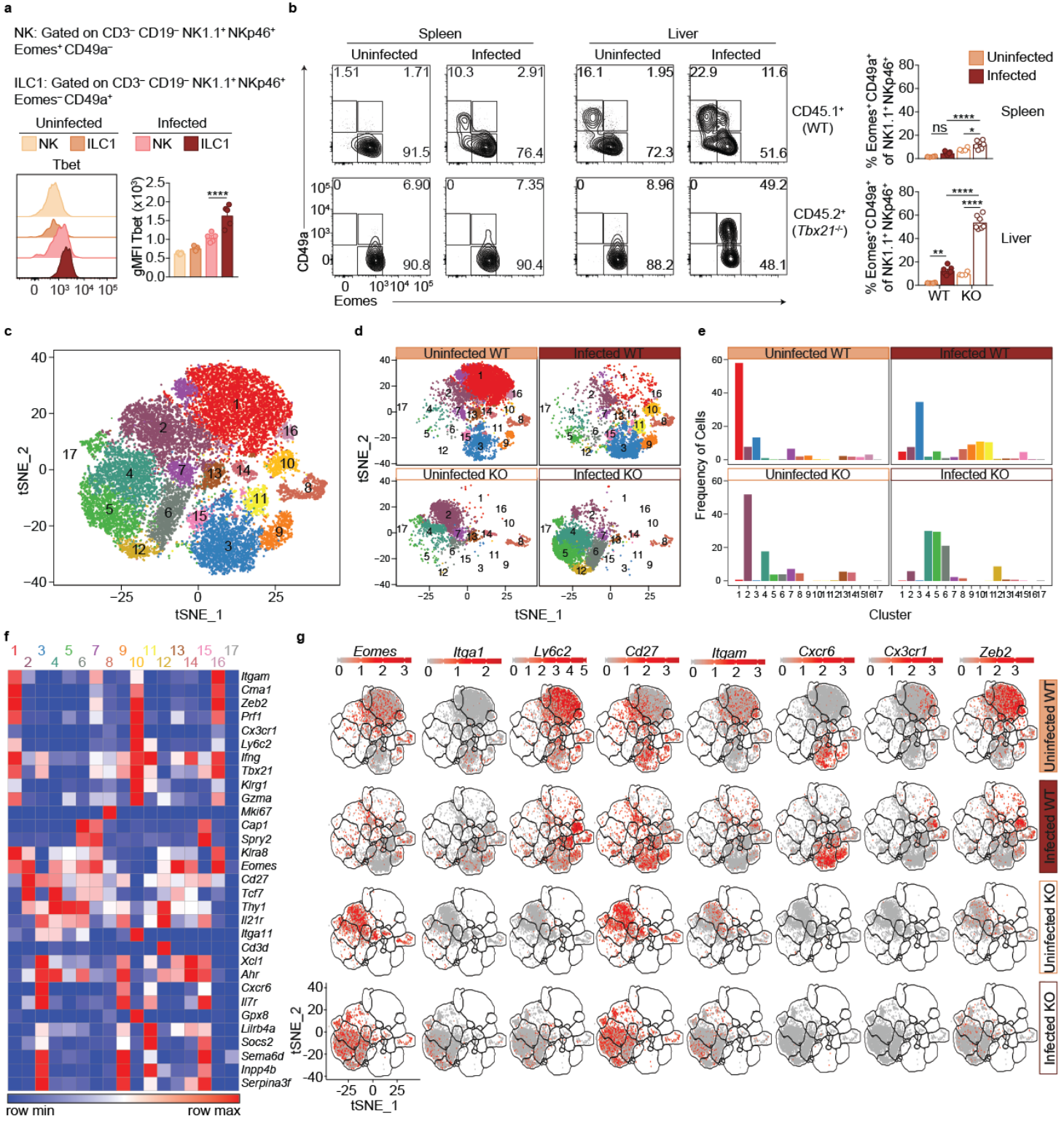
a
NK: Gated on CD3⁻ CD19⁻ NK1.1⁺ NKp46⁺ Eomes⁺ CD49a⁻
ILC1: Gated on CD3⁻ CD19⁻ NK1.1⁺ NKp46⁺ Eomes⁻ CD49a⁺
Uninfected
Infected
NK
ILC1
Tbet
gMFI Tbet (x10³)
****
b
Spleen
Liver
Uninfected
Infected
CD45.1⁺ (WT)
CD45.2⁺ (Tbx21⁻/⁻)
CD49a
Eomes
% Eomes⁺CD49a⁺ of NK1.1⁺NKp46⁺
ns
*
**
WT
KO
c
tSNE_1
tSNE_2
d
Uninfected WT
Infected WT
Uninfected KO
Infected KO
e
Frequency of Cells
Cluster
f
Itgam
Cma1
Zeb2
Prf1
Cx3cr1
Ly6c2
Ifng
Tbx21
Klrg1
Gzma
Mki67
Cap1
Spry2
Klra8
Eomes
Cd27
Tcf7
Thy1
Il21r
Itga11
Cd3d
Xcl1
Ahr
Cxcr6
Il7r
Gpx8
Lilrb4a
Socs2
Sema6d
Inpp4b
Serpina3f
row min
row max
g
Eomes
Itga1
Ly6c2
Cd27
Itgam
Cxcr6
Cx3cr1
Zeb2

Figure 6

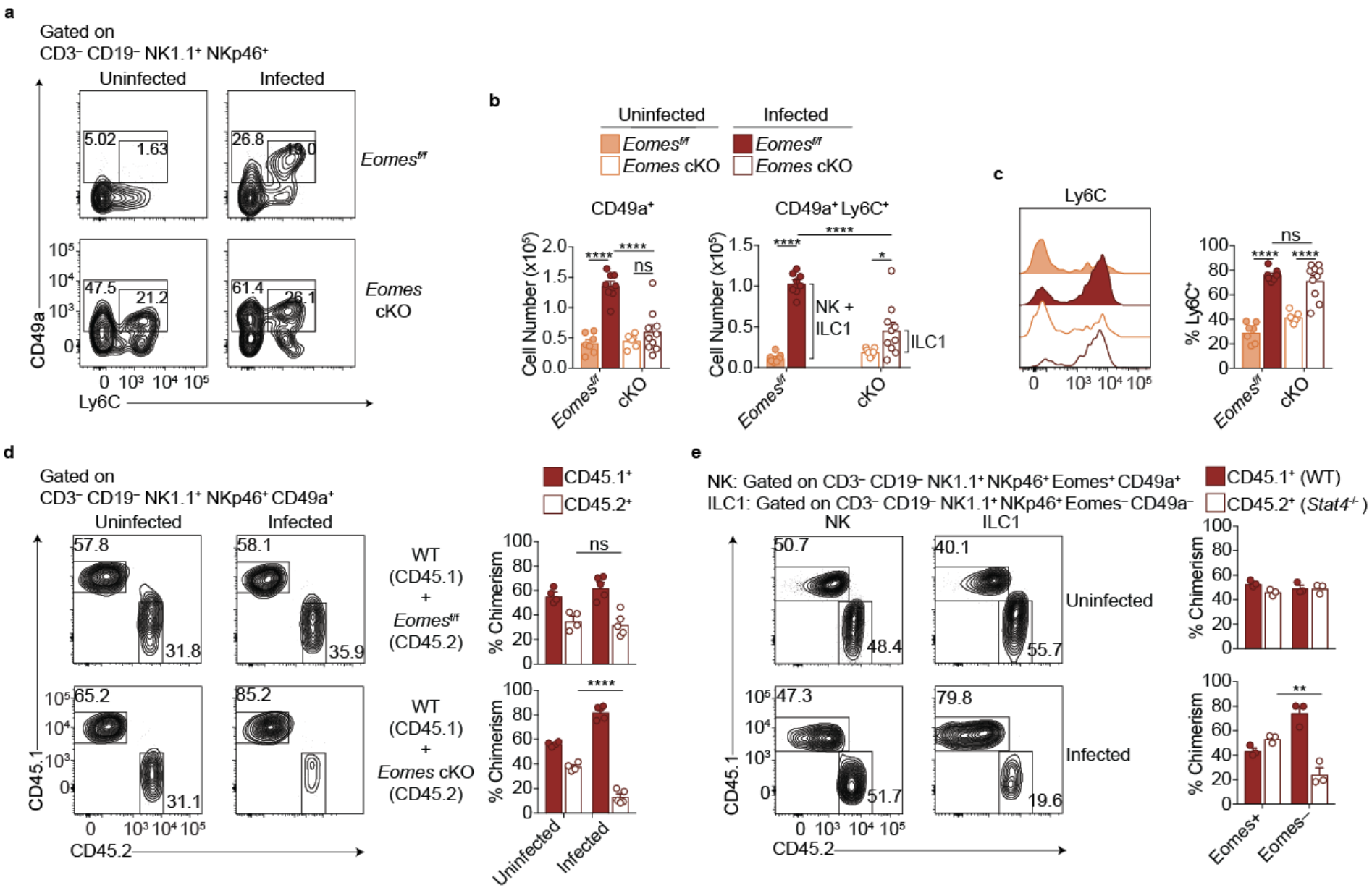
a
Gated on
CD3⁻ CD19⁻ NK1.1⁺ NKp46⁺
Uninfected
Infected
Eomes^f/f
Eomes cKO
CD49a
Ly6C
5.02
1.63
26.8
47.5
21.2
61.4
26.1
b
Uninfected
Infected
Eomes^f/f
Eomes cKO
CD49a⁺
CD49a⁺ Ly6C⁺
Cell Number (x10⁵)
NK + ILC1
ILC1
c
Ly6C
% Ly6C⁺
d
Gated on
CD3⁻ CD19⁻ NK1.1⁺ NKp46⁺ CD49a⁺
CD45.1⁺
CD45.2⁺
WT (CD45.1) + Eomes^f/f (CD45.2)
WT (CD45.1) + Eomes cKO (CD45.2)
CD45.1
CD45.2
% Chimerism
Uninfected
Infected
e
NK: Gated on CD3⁻ CD19⁻ NK1.1⁺ NKp46⁺ Eomes⁺ CD49a⁺
ILC1: Gated on CD3⁻ CD19⁻ NK1.1⁺ NKp46⁺ Eomes⁻ CD49a⁻
CD45.1⁺ (WT)
CD45.2⁺ (Stat4⁻/⁻)
NK
ILC1
Eomes+
Eomes–

Figure 7

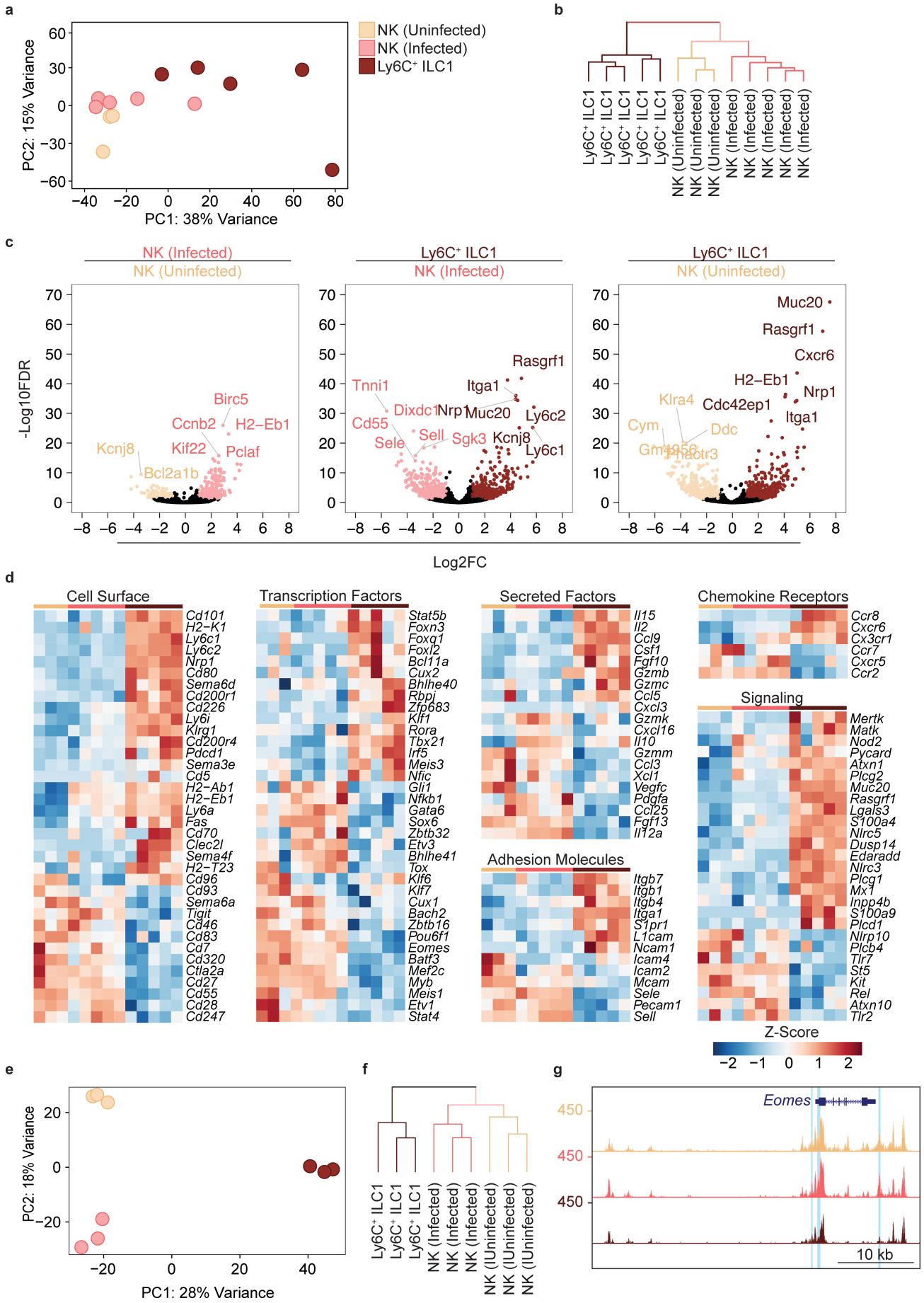
a
PC2: 15% Variance
PC1: 38% Variance
NK (Uninfected)
NK (Infected)
Ly6C⁺ ILC1
b
Ly6C⁺ ILC1
NK (Uninfected)
NK (Infected)
c
NK (Infected)
NK (Uninfected)
Ly6C⁺ ILC1
NK (Infected)
Ly6C⁺ ILC1
NK (Uninfected)
-Log10FDR
Log2FC
Birc5
Ccnb2
H2–Eb1
Kcnj8
Kif22
Pclaf
Bcl2a1b
Rasgrf1
Tnni1
Itga1
Dixdc1
Nrp1
Muc20
Ly6c2
Cd55
Sell
Sele
Sgk3
Kcnj8
Ly6c1
Muc20
Rasgrf1
Cxcr6
H2–Eb1
Nrp1
Klra4
Cdc42ep1
Itga1
Cym
Ddc
d
Cell Surface
Cd101
H2–K1
Ly6c1
Ly6c2
Nrp1
Cd80
Sema6d
Cd200r1
Cd226
Ly6i
Klrg1
Cd200r4
Pdcd1
Sema3e
Cd5
H2–Ab1
H2–Eb1
Ly6a
Fas
Cd70
Clec2l
Sema4f
H2–T23
Cd96
Cd93
Sema6a
Tigit
Cd46
Cd83
Cd7
Cd320
Ctla2a
Cd27
Cd55
Cd28
Cd247
Transcription Factors
Stat5b
Foxn3
Foxq1
Foxl2
Bcl11a
Cux2
Bhlhe40
Rbpj
Zfp683
Klf1
Rora
Tbx21
Irf5
Meis3
Nfic
Gli1
Nfkb1
Gata6
Sox6
Zbtb32
Etv3
Bhlhe41
Tox
Klf6
Klf7
Cux1
Bach2
Zbtb16
Pou6f1
Eomes
Batf3
Mef2c
Myb
Meis1
Etv1
Stat4
Secreted Factors
Il15
Il2
Ccl9
Csf1
Fgf10
Gzmb
Gzmc
Ccl5
Cxcl3
Gzmk
Cxcl16
Il10
Gzmm
Ccl3
Xcl1
Vegfc
Pdgfa
Ccl25
Fgf13
Il12a
Adhesion Molecules
Itgb7
Itgb1
Itgb4
Itga1
S1pr1
L1cam
Ncam1
Icam4
Icam2
Mcam
Sele
Pecam1
Sell
Chemokine Receptors
Ccr8
Cxcr6
Cx3cr1
Ccr7
Cxcr5
Ccr2
Signaling
Mertk
Matk
Nod2
Pycard
Atxn1
Plcg2
Muc20
Rasgrf1
Lgals3
S100a4
Nlrc5
Dusp14
Edaradd
Nlrc3
Plcg1
Mx1
Inpp4b
S100a9
Plcd1
Nlrp10
Plcb4
Tlr7
St5
Kit
Rel
Atxn10
Tlr2
Z-Score
e
PC2: 18% Variance
PC1: 28% Variance
f
Ly6C⁺ ILC1
NK (Infected)
NK (IUninfected)
g
Eomes
10 kb

Supplementary Fig 1

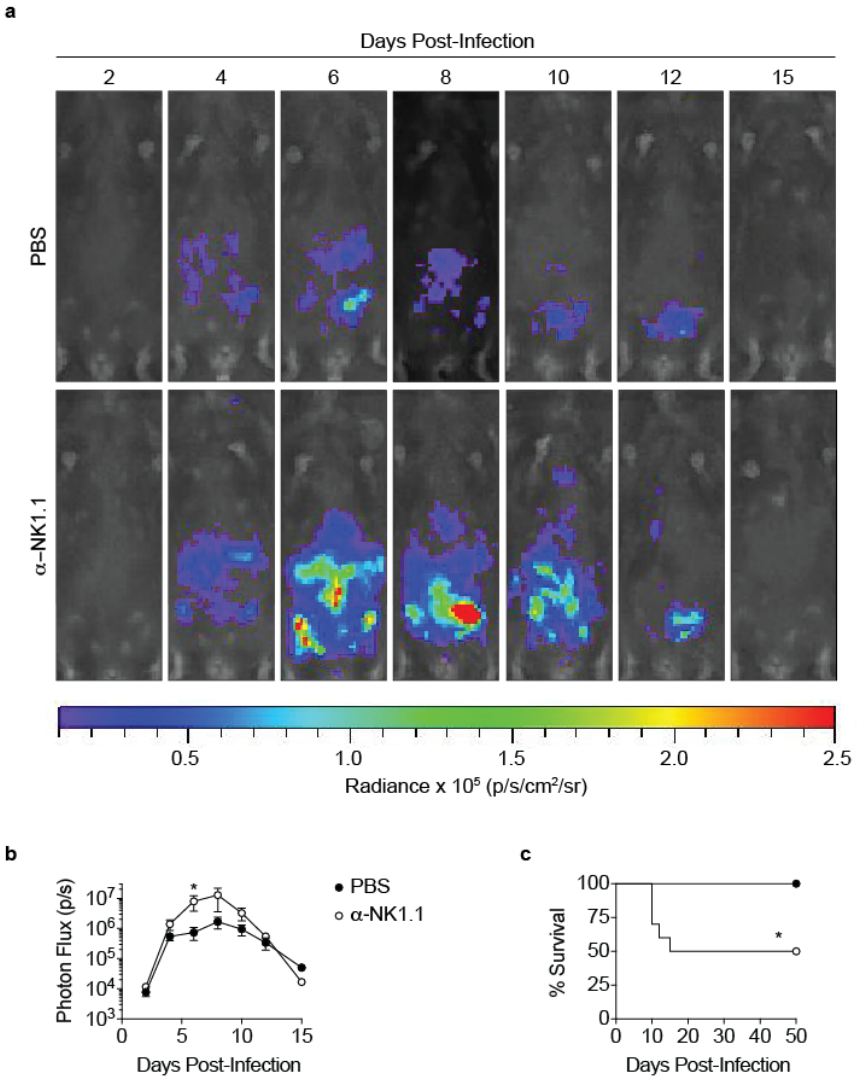

Supplementary Fig 2

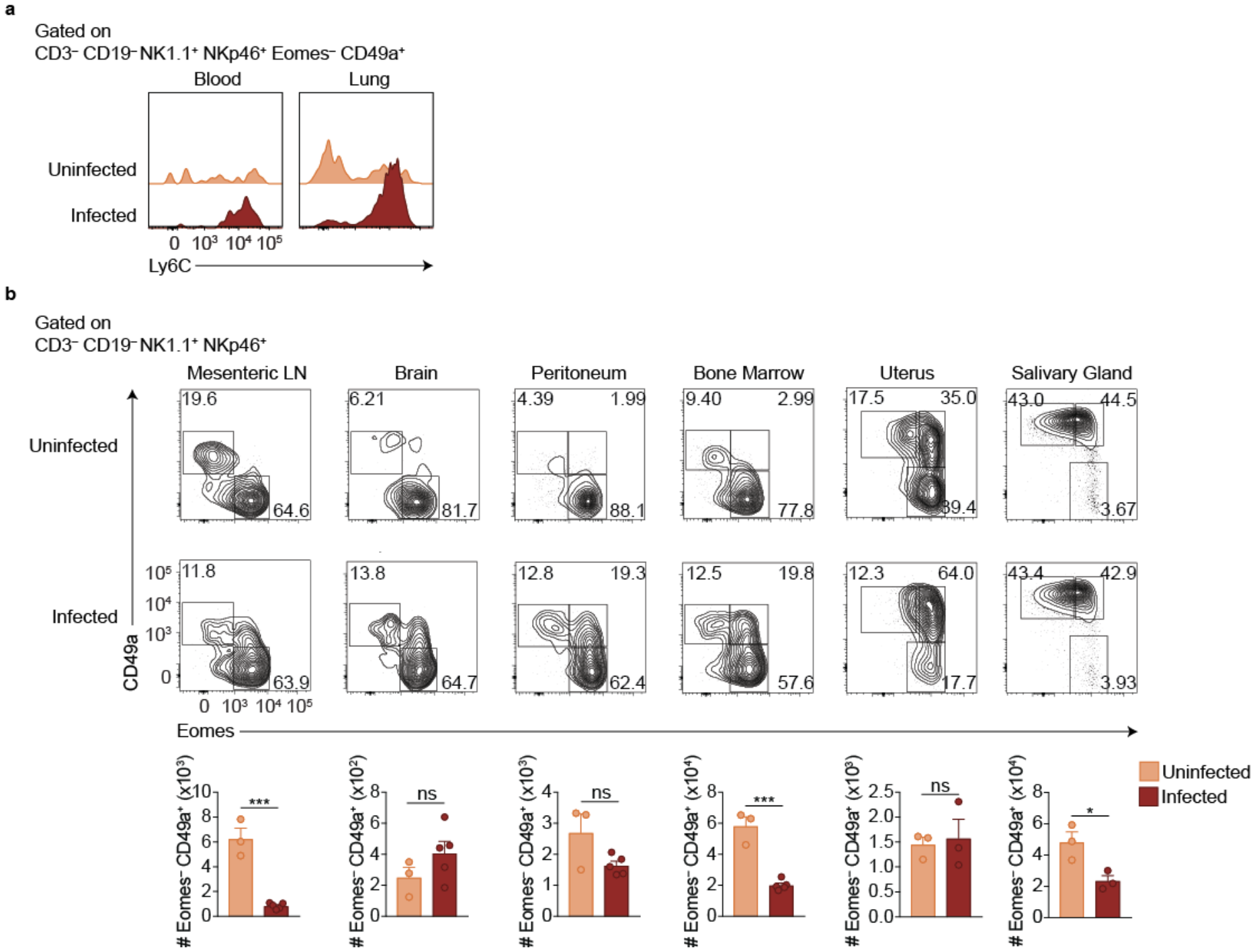

Supp Fig 3

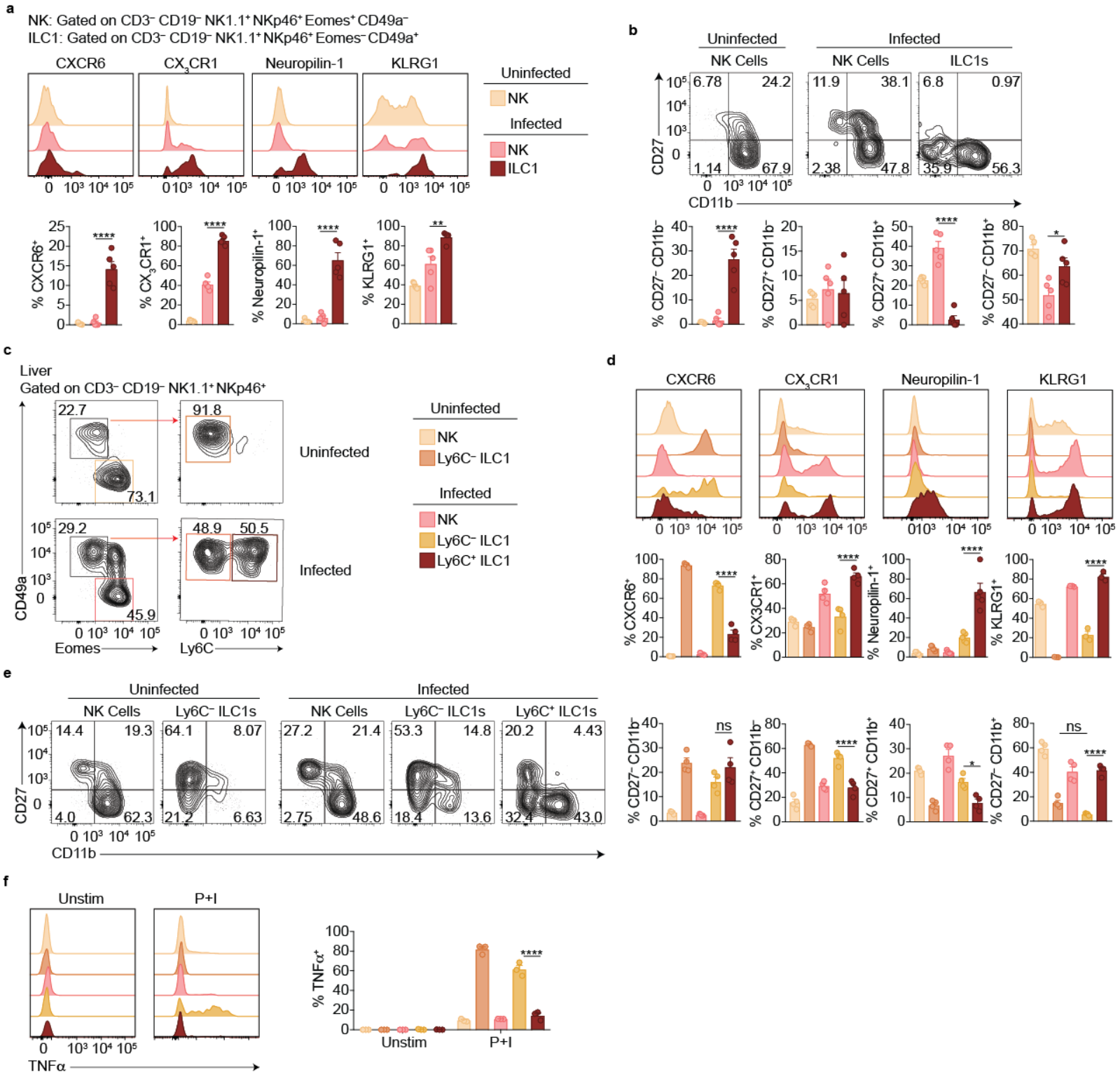
a
NK: Gated on CD3⁻ CD19⁻ NK1.1⁺ NKp46⁺ Eomes⁺ CD49a⁻
ILC1: Gated on CD3⁻ CD19⁻ NK1.1⁺ NKp46⁺ Eomes⁻ CD49a⁺
CXCR6
CX3CR1
Neuropilin-1
KLRG1
Uninfected
NK
Infected
NK
ILC1
% CXCR6⁺
% CX3CR1⁺
% Neuropilin-1⁺
% KLRG1⁺
b
Uninfected
Infected
NK Cells
NK Cells
ILC1s
6.78
24.2
1.14
67.9
11.9
38.1
2.38
47.8
6.8
0.97
35.9
56.3
CD27
CD11b
% CD27⁻ CD11b⁺
% CD27⁺ CD11b⁻
% CD27⁺ CD11b⁺
% CD27⁻ CD11b⁺
c
Liver
Gated on CD3⁻ CD19⁻ NK1.1⁺ NKp46⁺
22.7
73.1
91.8
29.2
45.9
48.9
50.5
Uninfected
Infected
CD49a
Eomes
Ly6C
Uninfected
NK
Ly6C⁻ ILC1
Infected
NK
Ly6C⁻ ILC1
Ly6C⁺ ILC1
d
CXCR6
CX3CR1
Neuropilin-1
KLRG1
% CXCR6⁺
% CX3CR1⁺
% Neuropilin-1⁺
% KLRG1⁺
e
Uninfected
Infected
NK Cells
Ly6C⁻ ILC1s
NK Cells
Ly6C⁻ ILC1s
Ly6C⁺ ILC1s
14.4
19.3
4.0
62.3
64.1
8.07
21.2
6.63
27.2
21.4
2.75
48.6
53.3
14.8
18.4
13.6
20.2
4.43
32.4
43.0
CD27
CD11b
% CD27⁻ CD11b⁺
% CD27⁺ CD11b⁻
% CD27⁺ CD11b⁺
% CD27⁻ CD11b⁺
ns
f
Unstim
P+I
TNFα
% TNFα⁺
Unstim
P+I

Suppl Fig 4

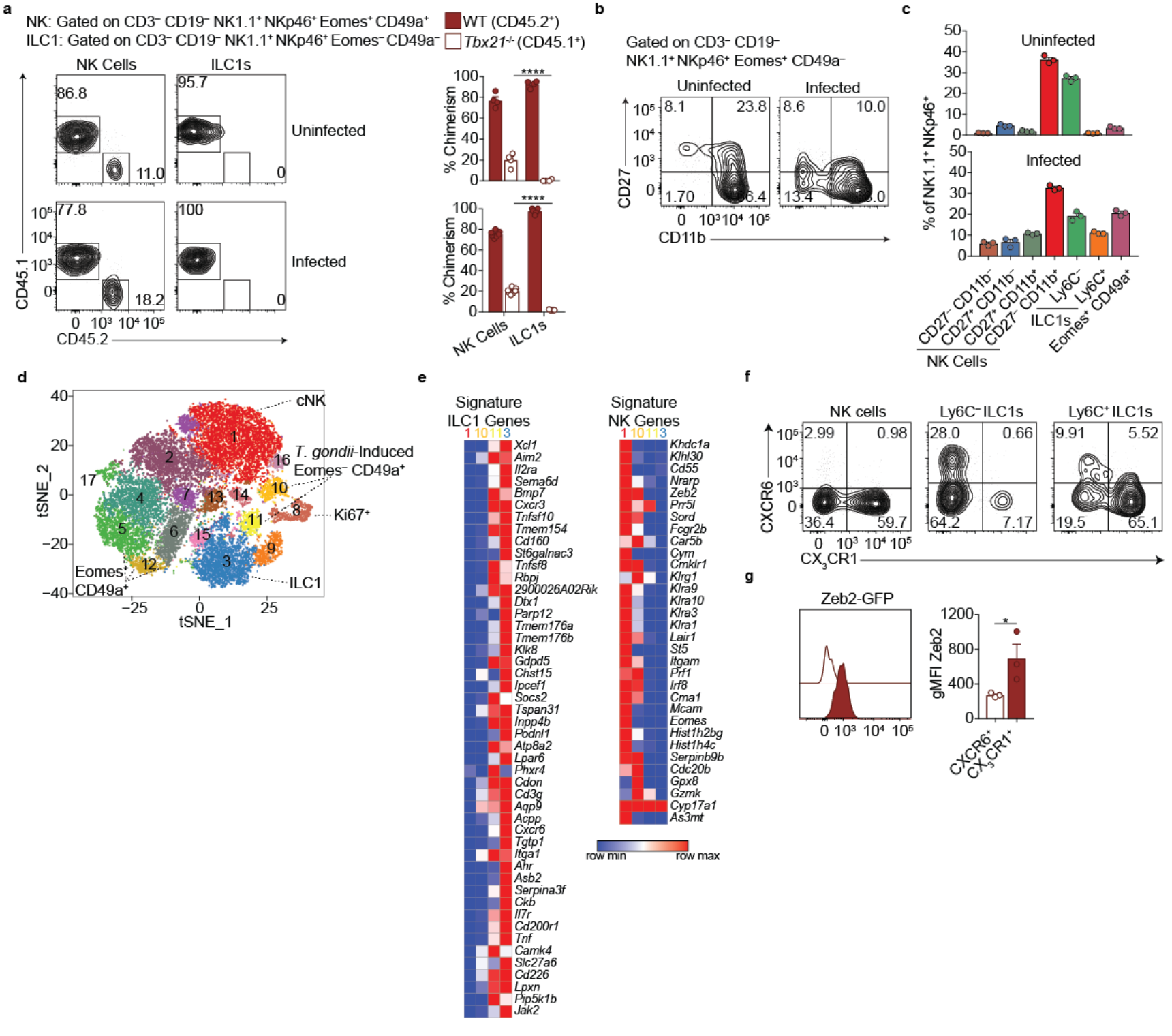
a
NK: Gated on CD3⁻ CD19⁻ NK1.1⁺ NKp46⁺ Eomes⁺ CD49a⁺
ILC1: Gated on CD3⁻ CD19⁻ NK1.1⁺ NKp46⁺ Eomes⁻ CD49a⁻
WT (CD45.2⁺)
Tbx21⁻/⁻ (CD45.1⁺)
NK Cells
ILC1s
Uninfected
Infected
CD45.1
CD45.2
% Chimerism
****
b
Gated on CD3⁻ CD19⁻
NK1.1⁺ NKp46⁺ Eomes⁺ CD49a⁻
Uninfected
Infected
CD27
CD11b
c
Uninfected
Infected
% of NK1.1⁺ NKp46⁺
CD27⁻ CD11b⁻
CD27⁺ CD11b⁻
CD27⁺ CD11b⁺
CD27⁻ CD11b⁺
Ly6C⁻
Ly6C⁺
Eomes⁺ CD49a⁺
NK Cells
ILC1s
d
cNK
T. gondii-Induced Eomes⁻ CD49a⁺
Ki67⁺
ILC1
Eomes⁺ CD49a⁺
tSNE_1
tSNE_2
e
Signature ILC1 Genes
Signature NK Genes
Xcl1
Aim2
Il2ra
Sema6d
Bmp7
Cxcr3
Tnfsf10
Tmem154
Cd160
St6galnac3
Tnfsf8
Rbpj
2900026A02Rik
Dtx1
Parp12
Tmem176a
Tmem176b
Klk8
Gdpd5
Chst15
Ipcef1
Socs2
Tspan31
Inpp4b
Podnl1
Atp8a2
Lpar6
Phxr4
Cdon
Cd3g
Aqp9
Acpp
Cxcr6
Tgtp1
Itga1
Ahr
Asb2
Serpina3f
Ckb
Il7r
Cd200r1
Tnf
Camk4
Slc27a6
Cd226
Lpxn
Pip5k1b
Jak2
Khdc1a
Klhl30
Cd55
Nrarp
Zeb2
Prr5l
Sord
Fcgr2b
Car5b
Cym
Cmklr1
Klrg1
Klra9
Klra10
Klra3
Klra1
Lair1
St5
Itgam
Prf1
Irf8
Cma1
Mcam
Eomes
Hist1h2bg
Hist1h4c
Serpinb9b
Cdc20b
Gpx8
Gzmk
Cyp17a1
As3mt
row min
row max
f
NK cells
Ly6C⁻ ILC1s
Ly6C⁺ ILC1s
CXCR6
CX3CR1
g
Zeb2-GFP
gMFI Zeb2
CXCR6⁺ CX3CR1⁺

Supplementary Fig 5

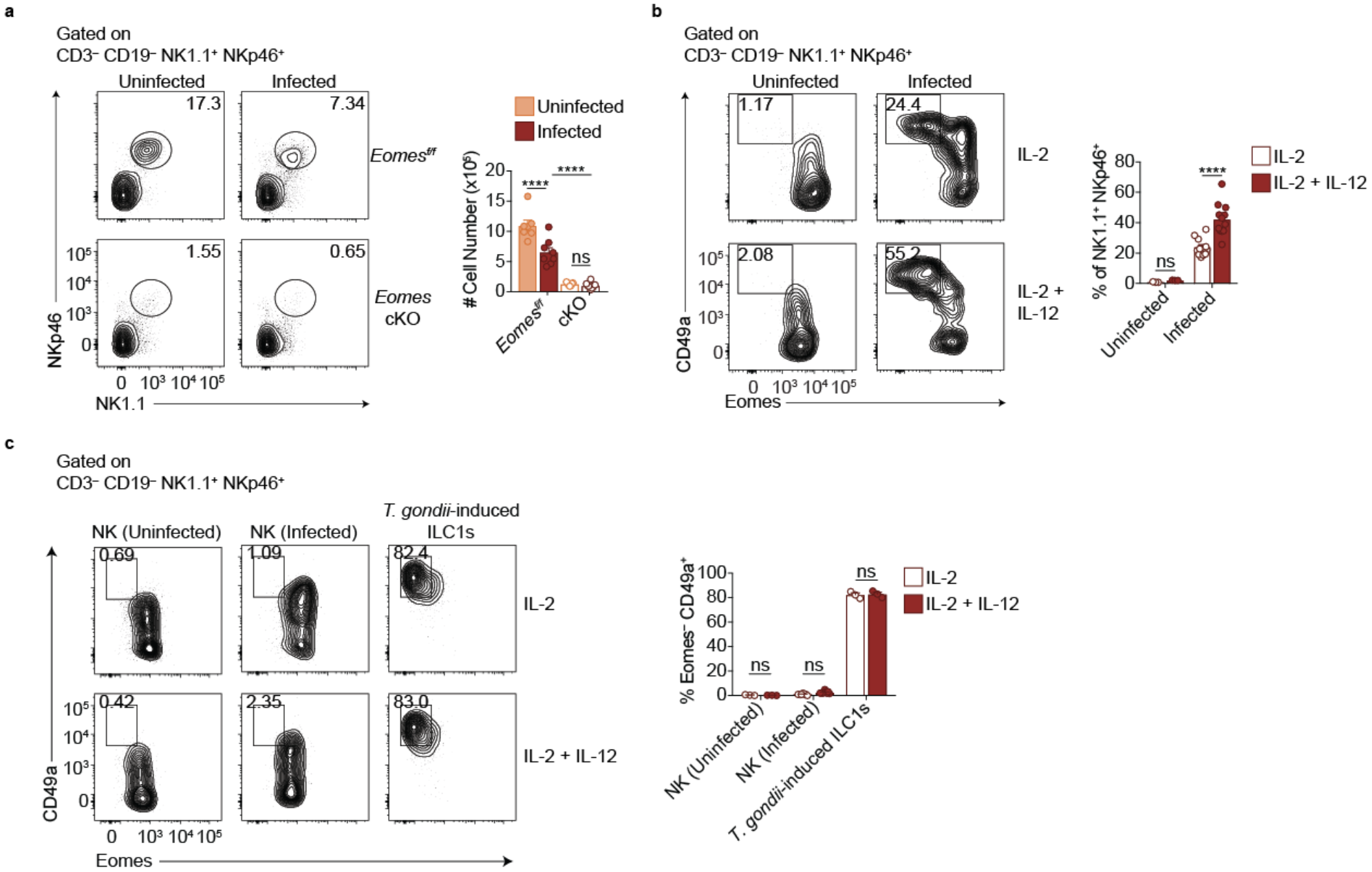

Suppl Fig 6

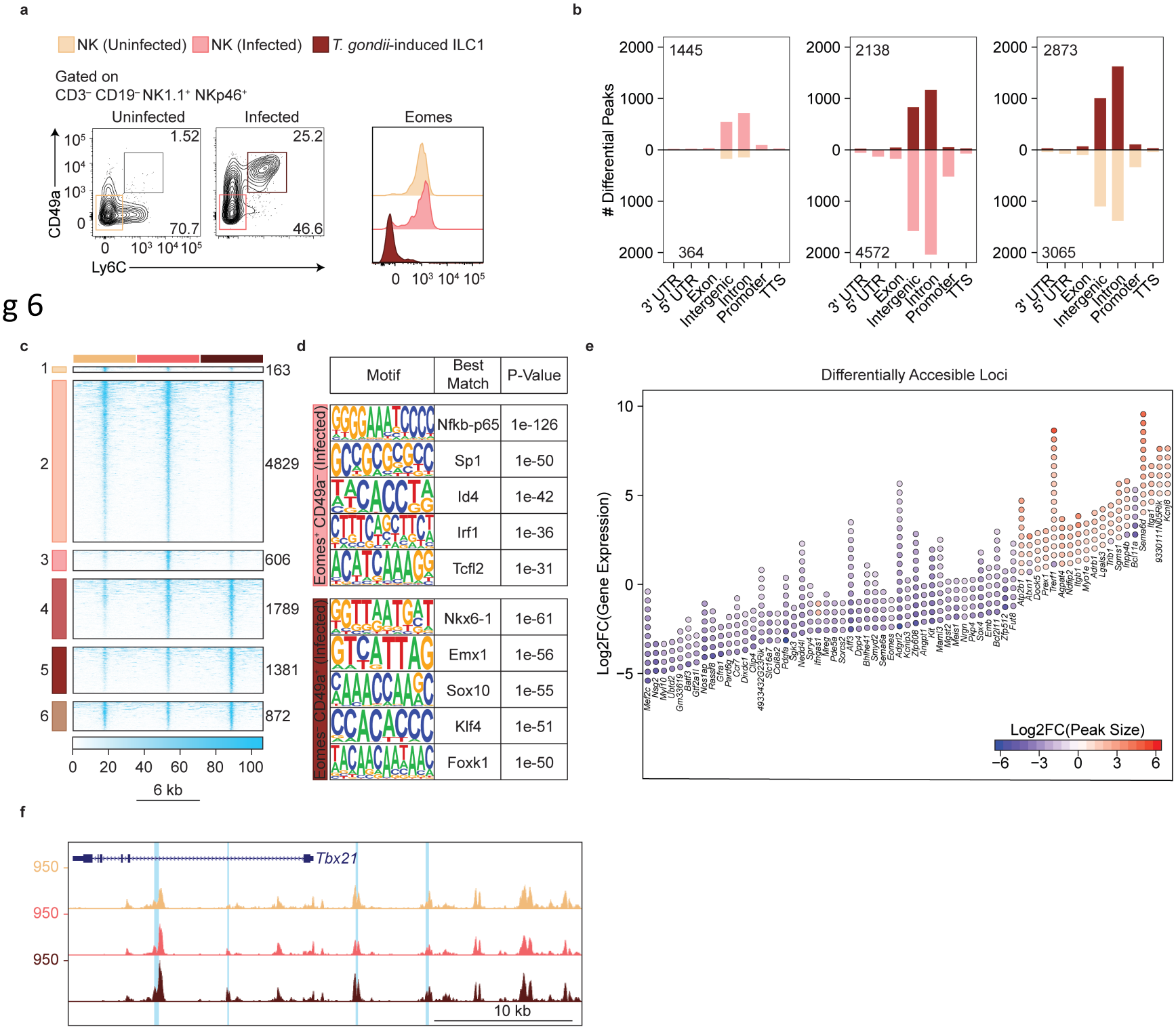
a
NK (Uninfected)
NK (Infected)
T. gondii-induced ILC1
Gated on
CD3⁻ CD19⁻ NK1.1⁺ NKp46⁺
Uninfected
Infected
Eomes
CD49a
Ly6C
1.52
70.7
25.2
46.6
b
Differential Peaks
1445
364
2138
4572
2873
3065
3' UTR
5' UTR
Exon
Intergenic
Intron
Promoter
TTS
c
163
4829
606
1789
1381
872
6 kb
d
Motif
Best Match
P-Value
Eomes⁺ CD49a⁻ (Infected)
Nfkb-p65 1e-126
Sp1 1e-50
Id4 1e-42
Irf1 1e-36
Tcfl2 1e-31
Eomes⁻ CD49a⁺ (Infected)
Nkx6-1 1e-61
Emx1 1e-56
Sox10 1e-55
Klf4 1e-51
Foxk1 1e-50
e
Differentially Accesible Loci
Log2FC(Gene Expression)
Log2FC(Peak Size)
f
Tbx21
10 kb